Response to Anonymous Referee #2's comments on "Analyses of Uncertainties and Scaling of Groundwater Level Fluctuations"

General comments:

1. *Liang and Zhang present an extension of previous work on the impact of temporal variations in hydrological processes on the uncertainty in groundwater level fluctuations. The authors derived analytical solutions for variance, covariance and spectrum of groundwater levels under random boundary conditions and a random source/sink, which is something new and interesting to the hydrological community.*

Response: Thank you for the positive comment by the reviewer on our study.

2. *The current work strongly relies on previous work of the same authors in that field, it can be interpreted as extension taking into account random boundary conditions and a random source/sink for a bounded groundwater flow model. Therefore, a technical note instead of a full research article appears to me the more appropriate form for publication.*

Response: We changed the type of this manuscript to a technical note.

3. *In this line, the section on Results and Discussion, especially section 3.1 could be shorted (specific comments later). Most of the publication is well-written, parts (in particular section 2 and 3.1) need to be improved in language, ideally by a native speaker.*

Response: We shortened the section 3.1 significantly based on the reviewer's specific suggestions and had a native speaker to edit and improve the writing of this revision.

4. *Figures and tables are in a good shape. However, the number of figures can be reduced by combining Figures 1+2 and Figures 3+4. I highly recommend to prepare an additional figure illustrating the one-dimensional groundwater flow model, including the nomenclature of the relevant processes (time-dependent source/sink, initial conditions, boundary conditions,...) for improving readability.*

Response: Thank you for your suggestions. We combined Figures 1and 2 as the new Figure 2 and combine Figures 3 and 4 as the new Figure 3.We added a new Figure 1to illustrate the conceptual model studied in response to both this and another reviewer's comment.

Specific comments:

Introduction

1. *p.3 l.1: What do you mean with "inherently erroneous"? The sentence could be misinterpreted.*

Response: To avoid misinterpretation, we replaced this sentence with "It is obvious that errors always exit in the groundwater levels calculated or simulated with analytical or numerical solutions. " in lines 51-52 of the revised manuscript.

2. *p.3 l.6-7: Please specify the sentence "The uncertainties in model parameters were investigated." (e.g. Which parameters? How?).*

   Response: We rewritten this sentence as "The uncertainties in the model parameters (e.g., hydraulic conductivity, recharge rate, evapotranspiration, and river conductance) were investigated based on generalized likelihood uncertainty estimation and Bayesian methods (Nowak et al., 2010;Neuman et al., 2012;Rojas et al., 2008;Rojas et al., 2010)" in lines 56-60 of the revised manuscript.

3. *p.3 l.11: Specify "Little attention" (Who?).*

   Response: We added corresponding citations, i.e., "Little attention has been given to the uncertainties in groundwater level due to temporal variations of hydrological processes, e.g., recharge, evapotranspiration, discharge to a river, and river stage (Bloomfield and Little, 2010;Zhang and Schilling, 2004;Schilling and Zhang, 2012;Liang and Zhang, 2013a;Zhu et al., 2012)" in lines 63-67 of the revised manuscript.

Formulation and solutions

4. *p.5 l6-7: Please elaborate more on the simplification of setting $H_0(x)$ to the steady state solution to the one-dimensional transient groundwater flow equation. Why is that an appropriate assumption?*

   Response: The initial condition has to be specified in order to solve the mathematical model. For a practical problem, the initial condition can be set based on real measurements or aquifer condition. Our study is theoretical with on real measurements and logical initial condition is a relative steady head distribution that is reached in an aquifer after a rainfall or during a wet season. The steady-state solution to this model was often adopted as the initial condition in previous research (Liang and Zhang, 2012, 2013a, b). Thus we set the initial condition $H_0(x)$ to be the steady-state solution to the one-dimensional groundwater flow equation. We elaborated this simplification in lines 116-124 of the revised manuscript.

5. *p.5 l.11-12: please explain this step on more detail.*

   Response: There were some typos in the original manuscript. We corrected them in lines 125 – 126 in the revised manuscript, i.e.,

   "Thus, the mean and perturbation of $H_0(x)$ can be written as,

   $\langle H_0(x)\rangle = h_0 + 0.5\langle W_0\rangle (L^2 - x^2)/T$ and $H_0{}'(x) = 0.5W_0^{'}(L^2 - x^2)/T$, respectively."

6. *p.6 l.11-12: Give a justification for the assumption of uncorrelated functions. How realistic is that assumption?*

   Response: This assumption may not be realistic. In general, W(t), Q(t), and H(t) should be correlated. It is possible to consider the relationship among W(t), Q(t), and H(t) by assuming some theoretical correlation functions but the problem is that 1) it is unclear what kind of correlation exists among these variable, 2) there is little observed data to support the type of the correlation assumed, and 3) simple analytical solutions would be difficulty to derive when considering the correlation . Therefore, we studied the case in which such correlation is weak in order to derive some simple analytical solutions. We believe this is an important first step towards solving this complex problem. and it also beyond the scopes of this paper and hope to relax this assumption in our future study.

7. *There are remarkable differences in the style and language of sections 3.1. and 3.2. To me, section 3.1 is much to circumstantial, where section 3.2 is more compact and to the point of interest. Therefore, section 3.1 should be shortened and adapted in style to that of section 3.2. Steps for improving the readability might be:*

• reducing doubling of explanations (e.g. p.9 l. 14/15) for all cases discussed
• not announcing the content of figures (e.g. p.9 l. 17 – p.14 l. 2) for all cases discussed. You may announce the visualization of results in Figure 1 at the beginning of the section and then directly refer to the Figure of interest, without repeating "The dimensionless standard deviation ... was presented in Figure 1...".
• Shortening aspects which can obviously be seen in the figure (e.g. p. 12. l. 3-6) "Similar to ...".
• Use a more compact description of the results (e.g. entire page 10).

Response: Thank you for the detailed comments to improve our manuscript. Based on your good suggestions we shortened section 3.1 significantly to make it more compact in the revised manuscript.

Conclusions

8. *p.17 l.10: What is a "typical aquifer studied"? Please formulate in a more generally way. If it is referred to the previous discussed example, please specify. (In general the conclusions drawn should be understandable without knowing details from the previous sections)*

Response: We added a note after “typical aquifer studied” to make this conclusion more clear in lines 376-378 in the revised manuscript, i.e., “In the typical sandy aquifer studied (with the length of aquifer at the direction of water flow L=100m, the average saturated thickness M =10m, hydraulic conductivity K=1m/day, and specific yield S_Y=0.25).”

9. *p.17 l.15: In both brackets it is stated "low frequencies".*

Response: We replaced first “low frequencies” with “high frequencies” in line 367 of the revised manuscript.

Figures and Tables

10. *Figure 1: The Figure is in general well constructed to show the different impacts of the processes. The readability of the figure and caption text could be improved by:*
• specifying the difference in the rows before ":(a) and (b)..." (e.g. by stating in the caption "for different combinations of ... (four rows) ")
• write the specific case to the figures (e.g. _2 W 6= 0 to Fig. 1c, etc.)
• The range of time values in Fig. 1b and 1d is different to those t values in Fig. 1f and 1h., where only the second range (those of 1f and 1h.) is state in the caption.

Response: We rewritten this figure caption and added specific text in each graphs according to your suggestion. We think it is clearer in revised manuscript.

11. *Figure 2: There is the same problem with values of t in Figure 2b and the caption.*
    Response: We revised it.

12. *Figure 2 should be combined with Figure 1, being sub-figures 1i and 1j.*
    Response: We did. Please see our response to your comment 4.

13. *Figure 4: Analogously to Figure 2, this Figure should be combined with Figure 3.*
    Response: We did. Please see our response to your comment 4.

Technical Corrections

14. *The text needs language improvements, ideally by a native speaker, in particular section 2 and 3.1.*
    Response: We had a native speaker to edit the manuscript. Please see our response to your comments 3.

15. *p.3 l.21: typo: "temporospatial"*
    Response: The word "temporospatial" should be allowed

16. p.9 l. 13: new paragraph starting.
    Response: We corrected it.

17. p.9 l.17: typo in σ_h'
    Response: We corrected it.

18. p.11 l. 6-8: Please rephrase. The sentence ("Unlike ...") is hardly understandable.
    Response: We rephrased the sentences in lines 222-226.

19. p.12 l.16: typo "settingσ"
    Response: We corrected it.

Technical note:

Analyses of Uncertainties and Scaling of Groundwater Level Fluctuations

Xiuyu Liang[a,b] , You-Kuan Zhang[a*,b,c]

[a]Center for Hydrosciences Research, Nanjing University,
Nanjing, Jiangsu 210093, P.R. China

[b]School of Earth Sciences and Engineering, Nanjing University,
Nanjing, Jiangsu 210093, P.R. China

[c]Department of Geoscience, University of Iowa,
Iowa City, Iowa 52242, USA

*Corresponding author
Phone: +86 25-83594485, Fax: +86 25-83596670,
Email: ykzhang@nju.edu.cn

Resubmitted to *Hydrology and Earth System Sciences*
May, 2015

Abstract

Analytical solutions for the variance, covariance, and spectrum of groundwater level, *h(x, t),* in an unconfined aquifer described by a linearized Boussinesq equation with random source/sink and initial and boundary conditions were derived. It was found that in a typical aquifer the error in *h(x, t)* in early time is mainly caused by the random initial condition and the error reduces as time progresses to reach a constant error in later time. The duration during which the effect of the random initial condition is significant may last a few hundred days in most aquifers. The constant error in *h(x, t)* in later time is due to the combined effects of the uncertainties in the source/sink and flux boundary: the closer to the flux boundary, the larger the error. The error caused by the uncertain head boundary is limited in a narrow zone near the boundary and remains more or less constant over time. The aquifer system behaves as a low-pass filter which filters out high-frequency noises and keeps low-frequency variations. Temporal scaling of groundwater level fluctuations exists in most part of a low permeable aquifer whose horizontal length is much larger than its thickness caused by the temporal fluctuations of areal source/sink.

Key words: Uncertainty of groundwater levels; Temporal scaling; Random source/sink; Random initial and boundary conditions.

1. Introduction

Groundwater level or hydraulic head (h) is the main driving force for water flow and advective contaminant transport in aquifers and thus the most important variable studied in groundwater hydrology and its applications. Knowledge about h is critical in dealing with groundwater-related environmental problems, such as over-pumping, subsidence, sea water intrusion, and contamination. One often found that the data about groundwater level is limited or unavailable in a hydrogeological investigation. In such cases the groundwater level distribution and its temporal variation are usually obtained with an analytical or numerical solution to a groundwater flow model.

It is obvious that errors always exit in the groundwater levels calculated or simulated with analytical or numerical solutions. The main sources of errors include the simplification or approximation in a conceptual model and the uncertainties in the model parameters. Problems in conceptualization or model structure were dealt with by many researchers (Neuman, 2003;Rojas et al., 2010;Ye et al., 2008;Rojas et al., 2008;Refsgaard et al., 2007;Zeng et al., 2013). The uncertainties in the model parameters (e.g., hydraulic conductivity, recharge rate, evapotranspiration, and river conductance) were investigated based on generalized likelihood uncertainty estimation and Bayesian methods (Nowak et al., 2010;Neuman et al., 2012;Rojas et al., 2008;Rojas et al., 2010). The uncertainty in groundwater level has been one of the main research topics in stochastic subsurface hydrology for more than three decades. Most of these studies were focused on the spatial variability of groundwater level due to aquifers' heterogeneity (Dagan, 1989;Gelhar, 1993;Zhang, 2002). Little attention has been given to the uncertainties in groundwater level due to temporal variations of hydrological processes, e.g., recharge, evapotranspiration, discharge to a river, and river stage (Bloomfield and Little, 2010;Zhang and Schilling, 2004;Schilling and Zhang, 2012;Liang and Zhang, 2013a;Zhu et al., 2012).

Uncertainties of groundwater level fluctuations have been studied by Zhang and Li (2005, 2006) and most recently by Liang and Zhang (2013a). Based on a linear reservoir model with a white noise or temporally-correlated recharge process, Zhang and Li (2005, 2006) derived the variance and covariance of $h(t)$ by considering only a random source or sink process assuming deterministic initial and boundary conditions. Liang and Zhang (2013a) extended the studies of Zhang and Li (2005, 2006) and carried out non-stationary spectral analysis and Monte Carlo simulations using a linearized Boussinesq equation, and investigated the temporospatial variations of groundwater level. However, the only random process considered by Liang and Zhang (2013a) is the source/sink. Temporal scaling of groundwater levels discovered first by Zhang and Schilling Zhang and Schilling (2004) was verified in several studies (Zhang and Li, 2005, 2006; Bloomfield and Little, 2010; Zhang and Yang, 2010; Zhu et al., 2012; Schilling and Zhang, 2012). However, we do not know the effect of random boundary conditions on temporal scaling of groundwater levels.

In this study we extended above-mentioned work by considering the groundwater flow in a bounded aquifer described by a linearized Boussinesq equation with a random source/sink as well as random initial and boundary conditions since the latter processes are known with uncertainties. The objectives of this study are 1) to derive analytical solutions for the covariance, variance and spectrum of groundwater level, and 2) to investigate the individual and combined effects of these random processes on uncertainties and scaling of $h(x, t)$. In the following we will first present the formulation and analytical solutions, then discuss the results, and finally draw some conclusions.

2. Formulation and Solutions

Under the Dupuit assumption, the one-dimensional transient groundwater flow in an unconfined aquifer near a river (Fig. 1) can be approximated with the linearized Boussinesq equation (Bear, 1972) with the initial and boundary conditions, i.e.,

$$T\frac{\partial^2 h}{\partial x^2}+W(t)=S_Y\frac{\partial h}{\partial t} \qquad (1a)$$

$$h(x,t)\big|_{t=0}=H_0(x); \qquad T\frac{\partial h}{\partial x}\bigg|_{x=0}=Q(t); \qquad h(x,t)\big|_{x=L}=H(t) \qquad (1b)$$

where T [L/T] is the transmissivity, h [L] is the hydraulic head or groundwater level above the bottom of the aquifer which is assumed to be horizontal, $W(t)$ [L/T] is the time-dependent source/sink term representing areal recharge or evapotranspiration, S_Y is the specific yield, $H_0(x)$ [L] is the initial condition, $Q(t)$ [L^2/T] is the time-dependent flux at the left boundary, $H(t)$ [L] is the time-dependent water level at the right boundary, L [L] is distance from the left to the right boundary, x [L] is the coordinate, and t [T] is time. In this study the initial head $H_0(x)$ is taken to be a spatially random variable, and the source/sink, $W(t)$, the flux to the left boundary, $Q(t)$, and the head at the right boundary, $H(t)$, are all taken to be temporally random processes and spatially deterministic. The parameters T and S_Y are taken to be constant.

The groundwater level, $h(x, t)$, the three random processes, $W(t)$, $Q(t)$, and $H(t)$, and the random variable, $H_0(x)$, are expressed in terms of their respective ensemble means plus small perturbations,

$$h(x,t) = \langle h(x,t) \rangle + h'(x,t) \tag{2a}$$

$$W(t) = \langle W(t) \rangle + W'(t); \qquad Q(t) = \langle Q(t) \rangle + Q'(t) \tag{2b}$$

$$H(t) = \langle H(t) \rangle + H'(t); \qquad H_0(x) = \langle H_0(x) \rangle + H_0'(x) \tag{2c}$$

where < > stands for ensemble average and ' for perturbation. The initial condition $H_0(x)$ in (1) can be any function. For the conceptualization of the groundwater flow presented in Fig. 1, the steady-state condition can be reached in this aquifer after a rainfall or during a wet season. Thus the steady-state solution to this model were often adopted as initial condition in previous research (Liang and Zhang, 2012, 2013a, b). Thus, in this study, we set initial condition $H_0(x)$ to be the steady-state solution to the one-dimensional groundwater flow equation, i.e., $H_0(x) = h_0 + 0.5W_0\left(L^2 - x^2\right)/T$, where h_0 [L] is the constant groundwater level at the right boundary and W_0 [L/T] is the spatially constant recharge rate (Liang and Zhang, 2012). Since h_0 is taken to be constant, the source of the uncertainty in the initial head $H_0(x)$ is due to random W_0 only. Thus, the mean and perturbation of $H_0(x)$ can be written as, $\langle H_0(x) \rangle = h_0 + 0.5\langle W_0 \rangle \left(L^2 - x^2\right)/T$ and $H_0'(x) = 0.5W_0'\left(L^2 - x^2\right)/T$, respectively. By substituting Eq. (2), $\langle H_0(x) \rangle$, and $H_0'(x)$ into Eq. (1) and taking expectation, one obtains the mean flow equation with the mean initial and boundary conditions as

$$T\frac{\partial^2 \langle h \rangle}{\partial x^2} + \langle W \rangle = S_Y \frac{\partial \langle h \rangle}{\partial t} \tag{3a}$$

$$\langle h(x,0)\rangle = h_0 + \frac{\langle W_0\rangle}{2T}\left(L^2 - x^2\right);\;\; T\frac{\partial\langle h\rangle}{\partial x}\Big|_{x=0} = \langle Q\rangle;\;\; \langle h(L,t)\rangle = \langle H(t)\rangle \tag{3b}$$

Subtracting Eq. (3) from (1) leads to the following perturbation equation with the initial and boundary conditions

$$T\frac{\partial^2 h'}{\partial x^2} + W' = S_Y \frac{\partial h'}{\partial t} \tag{4a}$$

$$h'(x,0) = \frac{W_0{}'}{2T}\left(L^2 - x^2\right);\quad T\frac{\partial h'}{\partial x}\Big|_{x=0} = Q';\;\; h'(L,t) = H'(t) \tag{4b}$$

The analytical solution to Eq. (4) can be derived with integral-transform methods (Ozisik, 1968) given by

$$h' = \frac{2}{L}\sum_{n=0}^{\infty} e^{-\beta b_n^2 t}\cos(b_n x)\left[\frac{(-1)^n}{b_n^3 T}W_0{}' + \beta\int_0^t e^{\beta b_n^2 \xi}\left[\frac{(-1)^n}{T b_n}W'(\xi) - \frac{Q'(\xi)}{T} + H'(\xi)(-1)^n b_n\right]d\xi\right] \tag{5}$$

where $\beta = T/S_Y$, $b_n = (2n+1)\pi/(2L)$. Using Eq. (5), the temporal covariance of the groundwater level fluctuations can be derived as

$$\begin{aligned} &C_{hh}(x,t_1;x,t_2) = E[h'(x,t_1)h'(x,t_2)] \\ &= \frac{4}{L^2}\sum_{m=0}^{\infty}\sum_{n=0}^{\infty} e^{-\beta\left(b_m^2 t_1 + b_n^2 t_2\right)}\cos(b_m x)\cos(b_n x)\left[\frac{(-1)^{m+n}}{T^2 b_m^3 b_n^3}\sigma_{W_0}^2\right. \\ &\left. + \beta^2 \int_0^{t_1}\int_0^{t_2} e^{\beta\left(b_m^2\xi + b_n^2\rho\right)}\left[\frac{(-1)^{n+m}}{T^2 b_m b_n}C_{WW}(\xi,\rho) + \frac{C_{QQ}(\xi,\rho)}{T^2} + C_{HH}(\xi,\rho)(-1)^{m+n} b_m b_n\right]d\xi d\rho\right] \end{aligned} \tag{6}$$

in which $\sigma_{W_0}^2$ is the variance of W_0, and $C_{WW}(\xi,\rho)$, $C_{QQ}(\xi,\rho)$ and $C_{HH}(\xi,\rho)$ are the temporal auto-covariance of *W(t)*, of *Q(t)*, and *H(t)*, respectively. We assume that *W(t)*, Q*(t)*, and *H(t)* are uncorrelated in order to simplify our analyses. It is shown in Eq. (6) that the head covariance depends on the variance of W_0 and the covariances of *W(t)*, Q*(t)*, and *H(t)* and this equation can be evaluated for any random *W(t)*, Q*(t)*, and *H(t)*. We assume that these processes are white noises as employed in previous studies (Gelhar, 1993;Hantush and Marino, 1994;Liang and Zhang, 2013a). More realistic randomness of these processes will be considered in future studies.

Following *Gelhar* (1993, p.34), we express the spectra of *W(t),* Q*(t),* and *H(t)* as $S_{WW} = \sigma_W^2 \lambda_W / \pi$, $S_{QQ} = \sigma_Q^2 \lambda_Q / \pi$, and $S_{HH} = \sigma_H^2 \lambda_H / \pi$, respectively, where σ_W^2, σ_Q^2, and σ_H^2 are the variances and λ_W, λ_Q, and λ_H are the correlation time intervals of these three processes, respectively. The corresponding covariance of *W(t), Q(t)* and *H(t)* are $C_{WW}(\xi,\rho) = 2\sigma_W^2 \lambda_W \delta(\xi-\rho)$, $C_{QQ}(\xi,\rho) = 2\sigma_Q^2 \lambda_Q \delta(\xi-\rho)$, and $C_{HH}(\xi,\rho) = 2\sigma_H^2 \lambda_H \delta(\xi-\rho)$. Substituting these covariance into (6) and taking integration, one obtain analytical solution of head covariance

$$C_{hh}(x',t',\tau') = \frac{4\beta L^2}{T^2} \sum_{m=0}^{\infty}\sum_{n=0}^{\infty} \cos(b'_m x')\cos(b'_n x') \left\{ e^{-\left[\left(b'^2_m + b'^2_n\right)t' + \left(b'^2_n - b'^2_m\right)\frac{\tau'}{2}\right]} \frac{L^2 (-1)^{m+n} \sigma_{W_0}^2}{\beta b'^3_m b'^3_n} + 2\frac{\left(e^{-b'^2_m \tau'} - e^{-2b'^2_m t'}\right)}{\left(b'^2_m + b'^2_n\right)} \left[\frac{(-1)^{m+n}\sigma_W^2 \lambda_W}{b'_m b'_n} + \frac{\sigma_Q^2 \lambda_Q}{L^2} + \frac{(-1)^{m+n} b'_m b'_n T^2 \sigma_H^2 \lambda_H}{L^4} \right] \right\} \quad (7)$$

where $\tau' = t'_2 - t'_1$ and $t' = (t'_2 + t'_1)/2$. The analytical solution for the head variance can be obtain by setting $\tau' = 0$

$$\sigma_h^2(x',t') = \frac{4\beta L^2}{T^2} \sum_{m=0}^{\infty}\sum_{n=0}^{\infty} \cos(b'_m x')\cos(b'_n x') \left\{ e^{-\left(b'^2_m + b'^2_n\right)t'} \frac{L^2}{\beta} \frac{(-1)^{m+n} \sigma_{W_0}^2}{b'^3_m b'^3_n} + 2\frac{1 - e^{-2b'^2_m t'}}{\left(b'^2_m + b'^2_n\right)} \left[\frac{(-1)^{m+n}\sigma_W^2 \lambda_W}{b'_m b'_n} + \frac{\sigma_Q^2 \lambda_Q}{L^2} + \frac{(-1)^{m+n} b'_m b'_n T^2 \sigma_H^2 \lambda_H}{L^4} \right] \right\} \quad (8)$$

where

$$t' = \frac{t}{t_c}; \quad x' = \frac{x}{L}; \quad t_c = \frac{L^2}{\beta}; \quad b'_n = \frac{(2n+1)\pi}{2}$$

in which $t_c (= S_Y L^2 / (KM))$ [1/T] is a characteristic timescale (Gelhar, 1993) where the transmissivity (*T*) is replaced by the product of the hydraulic conductivity (*K*) and the average saturated thickness (*M*) of the aquifer. The characteristic timescale (t_c) is an important parameter and its value for most shallow aquifers is usually larger than 100 day since the horizontal extent of a shallow aquifer is usually much larger than its thickness. For instance, the value of t_c is 250 days for a sandy aquifer with L=100m, M =10m, K=1m/day, and S_Y=0.25.

The spectral density of *h(x, t)* can't be derived by ordinary Fourier transform since the head covariance and variance depend on time *t'* and thus *h(x, t)* are temporally non-stationary as shown in Eqs. (7) and (8). Priestley (1981) defined the spectral density of non-stationary processes (Wigner spectrum) as the Fourier transform of time-dependent auto-covariance with fixed reference time *t* and derived time-dependent spectral density. In order to obtain the spectrum of *h(x, t)*, we applied Priestley's method and obtained the time-dependent spectral density (Priestley, 1981; Zhang and Li, 2005;Liang and Zhang, 2013a), i.e.,

$$
\begin{aligned}
S_{hh}(x,t,\omega) &= \frac{1}{2\pi}\int_{-\infty}^{\infty} C_{hh}(x,t,\tau)e^{-i\omega\tau}d\tau \\
&= \sum_{m=0}^{\infty}\sum_{n=0}^{\infty}\cos(b_m x)\cos(b_n x)\frac{2t_c\left(b_n^2-b_m^2\right)e^{-\beta\left(b_m^2+b_n^2\right)t}}{\beta^2\left(b_n^2-b_m^2\right)^2/4+\omega^2}\frac{(-1)^{m+n}\sigma_{W_0}^2}{\pi T^2 b_m^3 b_n^3}+ \\
&\quad \sum_{m=0}^{\infty}\sum_{n=0}^{\infty}\cos(b_m x)\cos(b_n x)\frac{8\beta b_m^2}{t_c\left(b_m^2+b_n^2\right)}\frac{1}{\beta^2 b_m^4+\omega^2}\left[\frac{(-1)^{m+n}S_{WW}}{T^2 b_m b_n}+\frac{S_{QQ}}{T^2}+(-1)^{m+n}b_m b_n S_{HH}\right]
\end{aligned} \tag{9}
$$

where ω is angular frequency and $\omega = 2\pi f$, f is frequency, and $i=\sqrt{-1}$. It is seen in Eq. (9) that the spectrum S_{hh} is dependent on not only frequency and locations but also time *t*. The time-dependent term (i.e., first term) in Eq. (9) is caused by the random initial condition and is proportional to $e^{-\beta\left(b_m^2+b_n^2\right)t}$ which decays quickly with *t*. We evaluated the first term in the Eq. (9) by setting *t*=0 and found that it is much smaller than the second term in Eq. (9). We thus ignored the first term and evaluated the spectrum using the approximation,

$$S_{hh}(x',\omega)=\sum_{m=0}^{\infty}\sum_{n=0}^{\infty}\frac{8\beta b'^2_m\cos(b'_m x')\cos(b'_n x')}{t_c\left(b'^2_m+b'^2_n\right)\left(\beta^2 b'^4_m/L^4+\omega^2\right)}\left[\frac{(-1)^{m+n}S_{WW}L^2}{T^2 b'_m b'_n}+\frac{S_{QQ}}{T^2}+\frac{(-1)^{m+n}b'_m b'_n S_{HH}}{L^2}\right] \tag{10}$$

3. Results and Discussion

3.1 Variance of groundwater levels

The general expression of the head variance in Eq. (8) depends on the variances of the four random processes, $\sigma^2_{W_0}$, σ^2_W, σ^2_Q, and σ^2_H. In the following we will study their individual and combined effects on the head variation and focus our attention only on the variance of *h(x, t)*. The dimensionless standard deviation of *h(x, t)*, σ'_h, or the square root of the dimensionless variance (σ'^2_h) as a function of the dimensionless time (*t'*) were evaluated and presented in the left column of Fig. 2 at fixed dimensionless locations (*x'*). The σ'_h as a function of *x'* was evaluated and presented in the right column of Fig. 2 at fixed *t'*.

We first evaluate the effect of the random initial condition due to the random term, W_0, by setting $\sigma^2_W=\sigma^2_Q=\sigma^2_H=0$. In this case the dimensionless variance in Eq. (8) reduces to

$$\sigma'^2_h(x',t')=\sum_{m=0}^{\infty}\sum_{n=0}^{\infty}\frac{(-1)^{m+n}}{b'^3_m b'^3_n}\cos(b'_m x')\cos(b'_n x')e^{-\left(b'^2_m+b'^2_n\right)t'} \tag{11}$$

where $\sigma'^2_h=\sigma^2_h T^2/(4L^4\sigma^2_{W_0})$. The changes of the σ'_h with *x'* and *t'* were presented in Fig 2a and 2b, respectively. It is shown in Fig. 2a that for a fixed location the σ'_h is at its maximum at *t'*=0 and decreases with time gradually to a negligible number at *t'*=1.0. This means that the error in *h(x, t)* predicted by an analytical or numerical solution due to the uncertain initial condition is significant at early time, especially near a flux boundary. The time duration during which the effect of the uncertain initial condition is significant depends on the value of the characteristic timescale (t_c) since $t' = t/t_c$. In the most aquifers this duration may last many days. In the typical aquifer studied the effect of the uncertainty in initial condition on *h(x, t)* is significant during first 250 days (t'=1.0). This duration should be relatively short, however, in a more permeable aquifer whose horizontal extent (*L*) is relatively smaller than its thickness (*M*). It is seen in Fig. 2b that for a fixed time, the σ'_h is the largest at the left flux boundary (x'=0.0) and becomes zero at the right constant head boundary (x'=1.0) since the right boundary is deterministic. This means that the error in *h(x, t)* predicted by an analytical or numerical solution due to the uncertain initial condition is significant almost everywhere in the aquifer: the further away from a constant head boundary, the larger the error.

We then consider the uncertainty in the areal source/sink term (*W*) by setting $\sigma^2_{W_0} = \sigma^2_Q = \sigma^2_H = 0$. In this case the dimensionless variance in Eq. (8) reduces to

$$\sigma'^2_h(x',t') = 2\sum_{m=0}^{\infty}\sum_{n=0}^{\infty}\cos(b'_m x')\cos(b'_n x')\frac{(1-e^{-2b'^2_m t'})(-1)^{m+n}}{(b'^2_m + b'^2_n)b'_m b'_n} \qquad (12)$$

where $\sigma'^2_h = \sigma^2_h T S_Y / (4L^2 \sigma^2_W \lambda_W)$. The changes of the σ'_h with x' and t' were presented in Fig 2c and 2d, respectively. It is noticed in Fig. 2c that at a fixed location, the σ'_h is zero initially, gradually increases as time goes, and approaches a constant limit at later time. This means that the error in *h(x, t)* due to an source/sink is at its minimum at early time and increases with time to approach a constant limit at later time: the closer to the left flux boundary, the larger the limit. For a fixed time the σ'_h decreases smoothly from the left to the right boundary (Fig. 2d). The error in *h(x,* *t)* due to the uncertainty in the source/sink is significant almost everywhere in the aquifer: the further away from the constant head boundary, the larger the error, similar to the previous case with the random initial condition (Fig. 2b).

Thirdly, we investigate the effect of the left random flux boundary by setting $\sigma_{W_0}^2 = \sigma_W^2 = \sigma_H^2 = 0$ in Eq. (8). In this case the dimensionless head variance is given by

$$\sigma'^2_h(x',t') = 2\sum_{m=0}^{\infty}\sum_{n=0}^{\infty}\cos(b'_m x')\cos(b'_n x')\frac{1-e^{-2b'^2_m t'}}{b'^2_m + b'^2_n} \qquad (13)$$

where $\sigma'^2_h = \sigma_h^2 T S_Y/(4\sigma_Q^2\lambda_Q)$. The changes of the σ'_h with *x'* and *t'* were presented in Fig 2e and 2f, respectively. At any location the σ'_h in Fig. 2e or the error in *h(x, t)* due to an uncertain flux boundary is at its minimum at early time and increases quickly with time to approach a constant limit: the closer to the left flux boundary, the larger the limit. At any time the σ'_h in Fig. 2f or the error in the head due to the uncertain flux boundary is at its maximum at the left boundary but decreases quickly away from the boundary to become insignificant for *x'*>0.8.

Fourthly, we investigated the effect of the random head boundary by setting $\sigma_{W_0}^2 = \sigma_W^2 = \sigma_Q^2 = 0$ in Eq. (8). The dimensionless head variance in this case is given by

$$\sigma'^2_h(x',t') = 2\sum_{m=0}^{\infty}\sum_{n=0}^{\infty}\cos(b'_m x')\cos(b'_n x')\frac{(-1)^{m+n} b'_m b'_n\left(1-e^{-2b'^2_m t'}\right)}{\left(b'^2_m + b'^2_n\right)} \qquad (14)$$

where $\sigma'^2_h = \sigma_h^2 L^2 S_Y/(4T\sigma_H^2\lambda_H)$. The changes of this σ'_h with *x'* and *t'* were presented in Fig 2g and 2h, respectively. It seen in Fig. 2g that at any location the σ'_h or the error in *h(x, t)* due to the random head boundary increases with time quickly to approach a constant limit: the closer to the uncertain head boundary, the larger the error. The spatial variation of σ'_h can be clearly observed in Fig. 2h for fixed *t'*. At any time σ'_h is at its maximum at the right boundary (*x'*=1) where the head is uncertain, decreases quickly away from the boundary. The error in *h(x, t)* due to the uncertain head boundary is limited in a narrow zone near the boundary (*x'*>0.8) (Fig. 2h).

Finally, we consider the combined effects of the uncertainties from all four sources, i.e., the initial condition, sources, and flux and head boundaries. The head variance in Eq. (8) is written in the dimensionless form as

$$\sigma'^2_h(x',t') = \sum_{m=0}^{\infty}\sum_{n=0}^{\infty}\cos(b'_m x')\cos(b'_n x')\left\{ e^{-\left(b'^2_m + b'^2_n\right)t'}\,\frac{(-1)^{m+n}\sigma'^2_{W_0}}{b'^3_m\, b'^3_n} + 2\frac{1-e^{-2b'^2_m t'}}{\left(b'^2_m + b'^2_n\right)}\left[\frac{(-1)^{m+n}}{b'_m\, b'_n} + \sigma'^2_Q + (-1)^{m+n} b'_m\, b'_n\, \sigma'^2_H\right]\right\} \tag{15}$$

where

$$\sigma'^2_h = \frac{\sigma_h^2 T S_Y}{4L^2\sigma_W^2\lambda_W};\quad \sigma'^2_{W_0} = \frac{L^2 S_Y \sigma^2_{W_0}}{T\sigma_W^2\lambda_W};\quad \sigma'^2_Q = \frac{\sigma_Q^2\lambda_Q}{L^2\sigma_W^2\lambda_W};\quad \sigma'^2_H = \frac{T^2\sigma_H^2\lambda_H}{L^4\sigma_W^2\lambda_W}$$

The dimensionless variances, $\sigma'^2_{W_0}$, σ'^2_Q and σ'^2_H, need to be specified in order to evaluate the dimensionless $\sigma'^2_h(x',t')$ in Eq. (15). For the typical aquifer mentioned above with *L*=100m, *T*=10 m^2/day (or *K*=1m/day and *M*=10m) and S_Y=0.25, we set $\sigma^2_{W_0}/(\sigma^2_W\lambda_W) = 10^{-1}$, $\sigma^2_Q\lambda_Q/(\sigma^2_W\lambda_W) = 10^3$, $\sigma^2_H\lambda_H/(\sigma^2_W\lambda_W) = 10^4$ and obtain $\sigma'^2_{W_0} = 25$, $\sigma'^2_Q = 0.1$ and $\sigma'^2_H = 0.01$.

The changes of this σ'_h with *x'* and *t'* were presented in Fig 2i and 2j, respectively. It is observed in Fig. 2i that at any location the σ'_h is at its maximum due to the uncertainty in the initial condition, gradually decreases as time goes, and approaches a constant limit at later time (t'>0.6) which is due to the combined effects of the uncertain source/sink and flux and head boundaries. This means that the error in the head in early time is significant if the initial condition is uncertain and reduces as time goes to reach a constant limit. The error in head in later time is determined by the uncertainties in the source/sink, flux and head boundaries. It can be observed in Fig. 2j that σ'_h is relatively larger near both boundaries. The values of σ'_h at the two boundaries are equivalent (~1.3) at early time, say t'=0.01 (the top curve in Fig. 2j) and it reduces slowly away from the flux boundary but quickly away from the head boundary. As time progresses, the σ'_h near the head boundary stays more or less the same but reduces significantly in most part of the aquifer. This means that in early time the error in *h(x, t)* in most part of the aquifer is mainly caused by the initial condition and at later time it is due to the combined effects of the uncertain areal source/sink and flux boundary. The effect of the uncertain head boundary on *h(x, t)* doesn't change with time significantly but is limited in a narrow zone near the boundary.

3.2 Spectrum of groundwater levels

We first evaluated S_{hh} in Eq. (10) due to the effect of the white noise flux boundary only by setting $S_{QQ} \neq 0$, $S_{WW} = 0$, and $S_{HH} = 0$. The dimensionless spectrum S_{hh}/S_{QQ} as a function of the frequency (*f*) was evaluated and presented in the log-log plot (Fig. 3a-3c) for three values of t_c (40, 400, and 4,000 days) since the value of t_c is 250 days for a sandy aquifer as we mentioned above and at the six locations (*x'* = 0.0, 0.2, 0.4, 0.6, 0.8, and 0.9). The spectrum S_{hh}/S_{QQ} in Fig. 3a is more or less horizontal (i.e., white noise) at low frequencies and decrease gradually as *f* increases, indicating that an aquifer acts as a low-bass filter that filter signals at high frequencies and keep signals at low frequencies. The aquifer has significantly dampened the fluctuations of the groundwater level. The spectrum varies with the location *x'*: the smaller the value of *x'* or the closer to the left flux boundary (*x'*=0), the larger the spectrum (Fig. 3a-3c). All spectra in Fig. 3a are not a straight line in the log-log plot, meaning that the temporal scaling of *h(x, t)* doesn't exist in the range of f =10^{-3}~10^{0} when t_c=40 days. As t_c increases to 400 and 4000 days, however, the spectrum at *x'*=0 become a straight line (the top curve in Fig. 3b and 3c) or has a power-law relation with *f*, i.e., $S_{hh}/S_{QQ} \propto 1/f$, since its slope is approximately one. The fluctuations of *h(0, t)* is a pink noise due to the white noise fluctuations flux boundary when the characteristic timescale (t_c) is large which means that the aquifer is relatively less permeable and/or has a much larger horizontal length than its thickness.

Secondly, the spectrum S_{hh}/S_{HH} due to the sole effect of the random head boundary was evaluated by setting $S_{HH} \neq 0$, $S_{WW} = 0$, and $S_{QQ} = 0$ in Eq. (10) for the same three values of t_c and six locations and presented in Fig. 3d-3f as a function of *f*. It is shown that similar to Fig. 3a-3c, the spectrum decreases as *f* increases but different from Fig. 3a-3c, the spectrum is larger at *x'*=0.9 near the right boundary (the top curves in Fig. 3d-3f) than that *x'*=0.0 (the bottom curves). Furthermore, none of the spectra are a straight line in the log-log plot, indicating that the temporal scaling of groundwater level fluctuations doesn't exist in the case of the white noise head boundary.

Thirdly, the spectrum S_{hh}/S_{WW} due the effect of the white noise recharge only was evaluated by setting $S_{WW} \neq 0$, $S_{QQ} = 0$, and $S_{HH} = 0$ in Eq. (10) for the same values of t_c and x' and presented in Fig. 3g-3i as a function of f. It is shown that when t_c=40 day the spectrum in Fig. 3g is horizontal at low frequencies and become a straight line at high frequencies: the closer to the right head boundary, the later it approaches a straight line (Fig. 3h). As t_c increases to 400 and 4000 days, the slope of the spectrum at all locations except at x'=0.9 approaches to a straight line with a slope of 2 (Fig. 3h and 3i), indicating a temporal scaling of $h(x, t)$. The fluctuations of groundwater level is a Brownian motion, i.e., $S \propto 1/f^2$, when $t_c \geq 4000$ day or in a relatively less permeable and/or has a much larger horizontal length than its thickness.

Finally, the head spectrum due to the combined effect of all three random sources (the white noise recharge, and flux and head boundaries) was evaluated, i.e., $S_{WW} \neq 0$, $S_{QQ} \neq 0$, and $S_{HH} \neq 0$ in Eq. (10). The spectrum of S_{hh}/S_{WW} as a function of f was presented in Fig. 3j-3l for the same values of t_c and x' where $S_{QQ}/S_{WW} = 1000$ and $S_{HH}/S_{WW} = 10000$ which are same with the values using in previous section. It is noticed that the general patterns of S_{hh}/S_{WW} in the combined case is similar to the case under the random source/sink only (Fig. 3g-3i) except at x'=0.0 and 0.9 (the dashed and dotted curves in Fig. 3j, respectively) due to the strong effects of the boundary conditions at these two locations. At t_c=4000 day, the spectra at all locations except *x'*=0.0 (Fig. 3l) are similar to those in Fig. 3i, indicating the dominating effect of the random areal source/sink. The spectrum at *x'*=0 in this case is also a straight line (the dashed curve in Fig. 3l) but with a different slope due to the effect of the random flux boundary which is similar to the top straight line in Fig. 3c. Above results provide a theoretical explanation as why temporal scaling exists in the observed groundwater level fluctuations (Zhang and Schilling, 2004;Bloomfield and Little, 2010;Zhu et al., 2012). We thus conclude that temporal scaling of *h(x, t)* may indeed exist in real aquifers due to the strong effect of the areal source/sink.

4. Conclusions

In this study the effects of random source/sink, and initial and boundary conditions on the uncertainty and temporal scaling of the groundwater level, *h(x, t)* were investigated. The analytical solutions for the variance, covariance and spectrum of *h(x, t)* in an unconfined aquifer described by a linearized Boussinesq equation with white noise source/sink, and initial and boundary conditions were derived. The standard deviations of *h(x, t)* for various cases were evaluated. Based on the results, the following conclusions can be drawn.

1. The error in *h(x, t)* due to a random initial condition is significant at early time, especially near a flux boundary. The duration during which the effect is significant may last a few hundred days in most aquifers;

2. The error in *h(x, t)* due to a random areal source/sink is significant in most part of an aquifer: the closer to a flux boundary, the larger the error;

3. The errors in $h(x, t)$ due to random flux and head boundaries are significant near the boundaries: the closer to the boundaries, the larger the errors. The random flux boundary may affect the head over a larger region near the boundary than the random head boundary;

4. In the typical sandy aquifer studied (with the length of aquifer at the direction of water flow L=100m, the average saturated thickness M =10m, hydraulic conductivity K=1m/day, and specific yield S_Y=0.25) the error in $h(x, t)$ in early time is mainly caused by an uncertain initial condition and the error reduces as time goes to reach a constant error in later time. The constant error in $h(x, t)$ is mainly due to the combined effects of uncertain source/sink and boundaries;

5. The aquifer system behaves as a low-pass filter which filter the short-term (high frequencies) fluctuations and keep the long-term (low frequencies) fluctuations;

6. Temporal scaling of groundwater level fluctuations may indeed exist in most part of a low permeable aquifer whose horizontal length is much larger than its thickness caused by the temporal fluctuations of areal source/sink.

Finally, it is pointed out that the analyses carried out in this study is under the assumptions that the processes, $W(t)$, $Q(t)$, and $H(t)$ are uncorrelated white noises. In reality, they may be correlated and spatially varied. We plan to relax those constrains and study more realistic cases in the near future. It is also noted that the analytical solutions for head variances derived in this study provide a way to identify and quantify the uncertainty. The spectrum relationship obtained among the head, recharge and boundary conditions can help one to improve spectrum analysis for a groundwater level time series and removed the effects of the boundary conditions.

Acknowledgment

This study was partially supported with the research grants from the National Nature Science Foundation of China (NSFC-41272260; NSFC-41330314; NSFC-41302180), the Natural Science Foundation of Jiangsu Province (SBK201341336) and from the National Key project "Water Pollution Control in the Huai River Basin" of China (2012ZX07204-001, 2012ZX07204-003).

References

Bear, J.: Dynamics of fluids in porous media, Environmental science series (New York, 1972-), American Elsevier Pub. Co., New York,, xvii, 764 p. pp., 1972.

Beven, K., and Binley, A.: The Future of Distributed Models - Model Calibration and Uncertainty Prediction, Hydrol Process, 6, 279-298, 1992.

Bloomfield, J. P., and Little, M. A.: Robust evidence for random fractal scaling of groundwater levels in unconfined aquifers, J Hydrol, 393, 362-369, DOI 10.1016/j.jhydrol.2010.08.031, 2010.

Dagan, G.: Flow and transport in porous formations, Springer-Verlag, Berlin ; New York, xvii, 465 p. pp., 1989.

Gelhar, L. W.: Stochastic subsurface hydrology, Prentice-Hall, Englewood Cliffs, N.J., x, 390 p. pp., 1993.

Hantush, M. M., and Marino, M. A.: One-Dimensional Stochastic-Analysis in Leaky Aquifers Subject to Random Leakage, Water Resour Res, 30, 549-558, Doi 10.1029/93wr02887, 1994.

Liang, X. Y., and Zhang, Y. K.: A new analytical method for groundwater recharge and discharge estimation, J Hydrol, 450, 17-24, DOI 10.1016/j.jhydrol.2012.05.036, 2012.

Liang, X. Y., and Zhang, Y. K.: Temporal and spatial variation and scaling of groundwater levels in a bounded unconfined aquifer, J Hydrol, 479, 139-145, DOI 10.1016/j.jhydrol.2012.11.044, 2013a.

Liang, X. Y., and Zhang, Y. K.: Analytic solutions to transient groundwater flow under time-dependent sources in a heterogeneous aquifer bounded by fluctuating river stage, Adv Water Resour, 58, 1-9, DOI 10.1016/j.advwatres.2013.03.010, 2013b.

Neuman, S. P.: Maximum likelihood Bayesian averaging of uncertain model predictions, Stoch Env Res Risk A, 17, 291-305, 10.1007/s00477-003-0151-7, 2003.

Neuman, S. P., Xue, L., Ye, M., and Lu, D.: Bayesian analysis of data-worth considering model and parameter uncertainties, Advances in Water Resources, 36, 75-85, 10.1016/j.advwatres.2011.02.007, 2012.

Nowak, W., de Barros, F. P. J., and Rubin, Y.: Bayesian geostatistical design: Task-driven optimal site investigation when the geostatistical model is uncertain, Water Resour Res, 46, Artn W03535 Doi 10.1029/2009wr008312, 2010.

Priestley, M. B.: Spectral Analysis and Time Series, Academic Press, San Diego, 1981.

Refsgaard, J. C., van der Sluijs, J. P., Hojberg, A. L., and Vanrolleghem, P. A.: Uncertainty in the environmental modelling process - A framework and guidance, Environmental Modelling & Software, 22, 1543-1556, 10.1016/j.envost.2007.02.004, 2007.

Rojas, R., Feyen, L., and Dassargues, A.: Conceptual model uncertainty in groundwater modeling: Combining generalized likelihood uncertainty estimation and Bayesian model averaging, Water Resources Research, 44, 10.1029/2008wr006908, 2008.

Rojas, R., Feyen, L., Batelaan, O., and Dassargues, A.: On the value of conditioning data to reduce conceptual model uncertainty in groundwater modeling, Water Resources Research, 46, 20, 10.1029/2009wr008822, 2010.

Schilling, K. E., and Zhang, Y. K.: Temporal Scaling of Groundwater Level Fluctuations Near a Stream, Ground Water, 50, 59-67, DOI 10.1111/j.1745-6584.2011.00804.x, 2012.

Vrugt, J. A., Gupta, H. V., Bouten, W., and Sorooshian, S.: A Shuffled Complex Evolution Metropolis algorithm for optimization and uncertainty assessment of hydrologic model parameters, Water Resources Research, 39, 10.1029/2002wr001642, 2003.

Ye, M., Meyer, P. D., and Neuman, S. P.: On model selection criteria in multimodel analysis, Water Resources Research, 44, 10.1029/2008wr006803, 2008.

Zeng, X. K., Wang, D., Wu, J. C., and Chen, X.: Reliability Analysis of the Groundwater Conceptual Model, Human and Ecological Risk Assessment, 19, 515-525, 10.1080/10807039.2012.713822, 2013.

Zhang, D.: Stochastic methods for flow in porous media : coping with uncertainties, Academic, San Diego, Calif. London, xiv, 350 p. pp., 2002.

Zhang, Y. K., and Schilling, K.: Temporal scaling of hydraulic head and river base flow and its implication for groundwater recharge, Water Resour Res, 40, -, Artn W03504 Doi 10.1029/2003wr002094, 2004.

Zhang, Y. K., and Li, Z. W.: Temporal scaling of hydraulic head fluctuations: Nonstationary spectral analyses and numerical simulations, Water Resources Research, 41, 10.1029/2004wr003797, 2005.

Zhang, Y. K., and Li, Z. W.: Effect of temporally correlated recharge on fluctuations of groundwater levels, Water Resources Research, 42, 10.1029/2005wr004828, 2006.

Zhang, Y. K., and Yang, X. Y.: Effects of variations of river stage and hydraulic conductivity on temporal scaling of groundwater levels: numerical simulations, Stoch Env Res Risk A, 24, 1043-1052, DOI 10.1007/s00477-010-0437-5, 2010.

Zhu, J. T., Young, M. H., and Osterberg, J.: Impacts of riparian zone plant water use on temporal scaling of groundwater systems, Hydrol Process, 26, 1352-1360, Doi 10.1002/Hyp.8241, 2012.

Figure captions

Figure 1 A schematic of the unconfined aquifer studied where $W(t)$ is the random time-dependent source/sink, $H_0(x)$ is the random initial condition, $Q(t)$ is the random time-dependent flux at the left boundary, $H(t)$ is the random time-dependent water level at the right boundary, L is distance from the left to the right boundary, and $h(x, t)$ is the random groundwater level in the aquifer.

Figure 2 The graphs on the left column are the standard deviation (σ'_h) of groundwater level ($h(x, t)$) versus the dimensionless time (t') at the dimensionless locations x'=0.0, 0.2, 0.4, 0.6, and 0.8. The graphs on the right column are σ'_h versus x' for the different t': b) and d) are for t'= 0.0, 0.2, 0.4, 0.6 and 0.8, f) and h) are for t'=0.01, 0.1, and 1.0, and j) is for t'=0.01, 0.2, 0.4, 0.6 and 0.8. Also, a) and b) are based on Eq.(11) where $\sigma_W^2 = \sigma_Q^2 = \sigma_H^2 = 0$; c) and d) are based on Eq. (12) where $\sigma_{W_0}^2 = \sigma_Q^2 = \sigma_H^2 = 0$; e) and f) are based on Eq. (13) where $\sigma_{W_0}^2 = \sigma_W^2 = \sigma_H^2 = 0$; g) and h) are based on Eq. (14) where $\sigma_{W_0}^2 = \sigma_W^2 = \sigma_Q^2 = 0$; i) and j) are based on Eq.(15) where $\sigma_{W_0}^2 \neq \sigma_W^2 \neq \sigma_Q^2 \neq \sigma_H^2 \neq 0$.

Figure 3 The dimensionless power spectrum versus frequency (f) at the dimensionless locations x'=0.0, 0.2, 0.4, 0.6, 0.8, and 0.9. The graphs on the left column are for t_c = 40 day, the graphs on the middle column are for t_c = 400 day, and the graphs on the right column are for t_c = 4000 day. The graphs on the first row are the dimensionless spectrum S_{hh}/S_{QQ} when $S_{WW} = 0$, $S_{HH} = 0$, and $S_{QQ} \neq 0$ in Eq. (10), the graphs on the second row is S_{hh}/S_{HH} when $S_{WW} = 0$, $S_{QQ} = 0$, and $S_{HH} \neq 0$, the graphs on the third row are S_{hh}/S_{WW} when $S_{QQ} = 0$, $S_{HH} = 0$, and $S_{WW} \neq 0$, and the graphs on the bottom row is S_{hh}/S_{WW} when $S_{QQ} \neq 0$, $S_{HH} \neq 0$, and $S_{WW} \neq 0$.

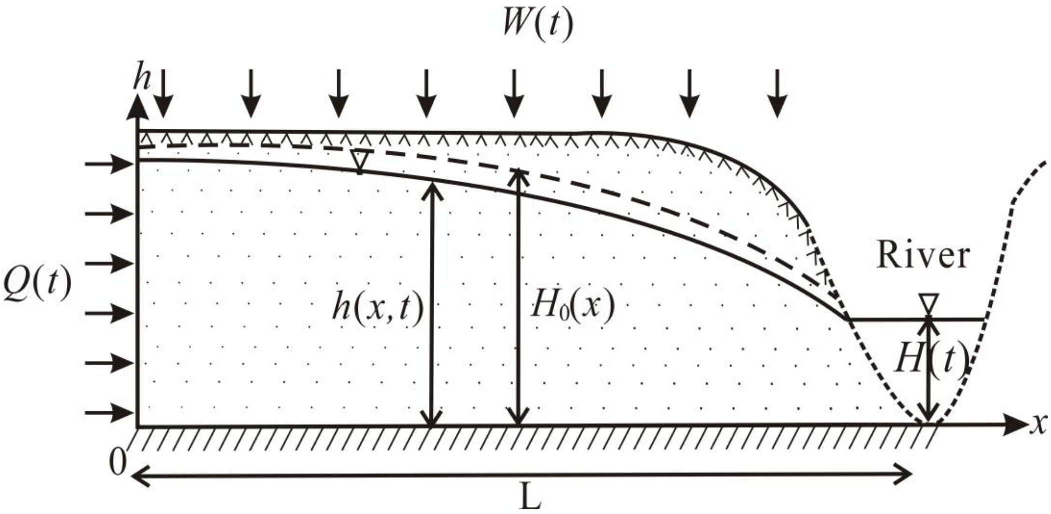

Figure 1

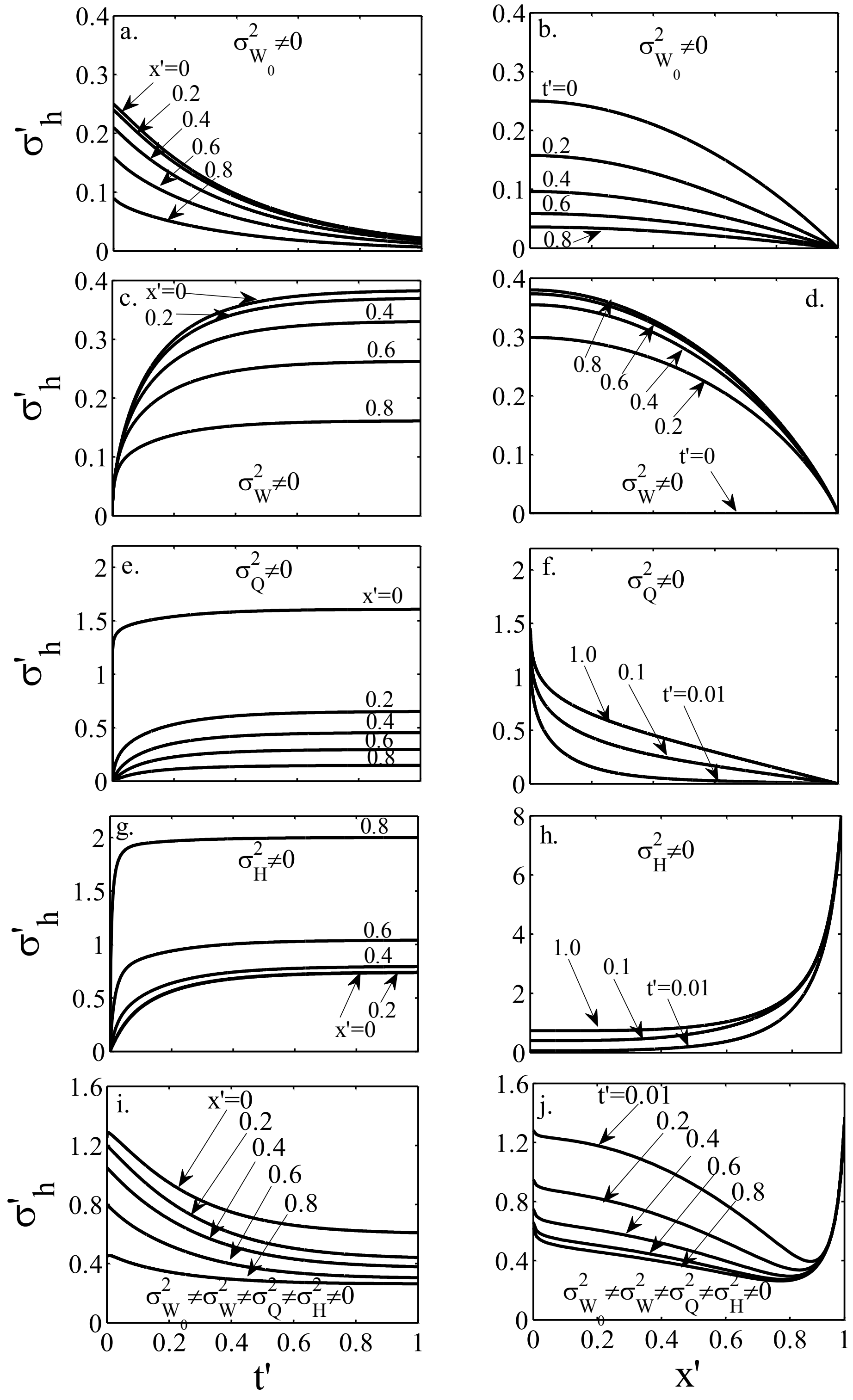

a.
$\sigma^2_{W_0} \neq 0$
x'=0
0.2
0.4
0.6
0.8
b.
$\sigma^2_{W_0} \neq 0$
t'=0
0.2
0.4
0.6
0.8
c.
x'=0
0.2
0.4
0.6
0.8
$\sigma^2_W \neq 0$
d.
0.8
0.6
0.4
0.2
t'=0
$\sigma^2_W \neq 0$
e.
$\sigma^2_Q \neq 0$
x'=0
0.2
0.4
0.6
0.8
f.
$\sigma^2_Q \neq 0$
1.0
0.1
t'=0.01
g.
$\sigma^2_H \neq 0$
0.8
0.6
0.4
0.2
x'=0
h.
$\sigma^2_H \neq 0$
1.0
0.1
t'=0.01
i.
x'=0
0.2
0.4
0.6
0.8
$\sigma^2_{W_0} \neq \sigma^2_W \neq \sigma^2_Q \neq \sigma^2_H \neq 0$
j.
t'=0.01
0.2
0.4
0.6
0.8
$\sigma^2_{W_0} \neq \sigma^2_W \neq \sigma^2_Q \neq \sigma^2_H \neq 0$
σ'_h
t'
x'

Figure 2

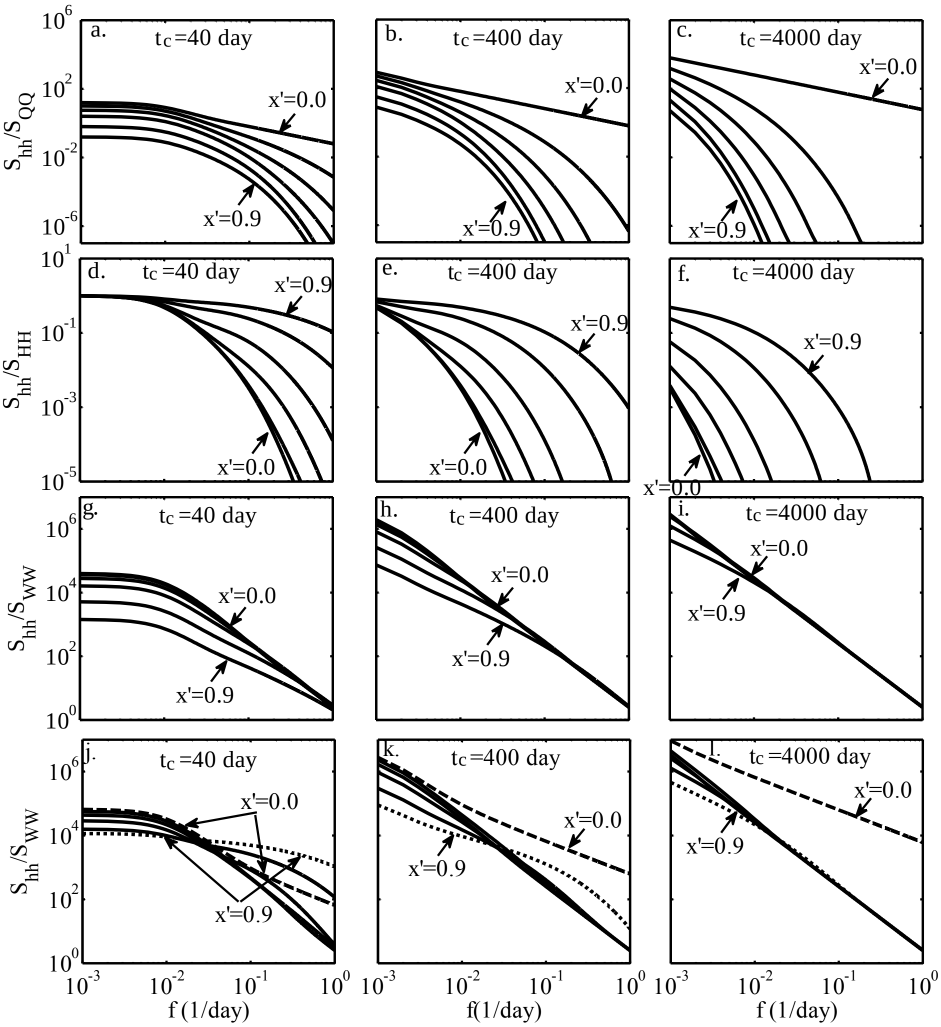
a.
b.
c.
d.
e.
f.
g.
h.
i.
j.
k.
l.
t_c =40 day
t_c =400 day
t_c =4000 day
x'=0.0
x'=0.9
S_{hh}/S_{QQ}
S_{hh}/S_{HH}
S_{hh}/S_{WW}
f (1/day)
f(1/day)

Figure 3

Technical note:

带格式的：字体：加粗，倾斜

带格式的：字体：加粗，倾斜

Analyses of Uncertainties and Scaling of Groundwater Level Fluctuations

Xiuyu Liang[a,b] , You-Kuan Zhang[a*,b,c]

[a]Center for Hydrosciences Research, Nanjing University,
Nanjing, Jiangsu 210093, P.R. China

[b]School of Earth Sciences and Engineering, Nanjing University,
Nanjing, Jiangsu 210093, P.R. China

[c]Department of Geoscience, University of Iowa,
Iowa City, Iowa 52242, USA

*Corresponding author
Phone: +86 25-83594485, Fax: +86 25-83596670,
Email: ykzhang@nju.edu.cn

~~Submitted~~ Resubmitted to *Hydrology and Earth System Sciences*

~~November~~May, ~~2014~~2015

Abstract

Analytical solutions for the variance, covariance, and spectrum of groundwater level, *h(x, t),* in an unconfined aquifer described by a linearized Boussinesq equation with random source/sink and initial and boundary conditions were derived. It was found that in a typical aquifer the error in *h(x, t)* in early time is mainly caused by the random initial condition and the error reduces as time progresses to reach a constant error in later time. The duration during which the effect of the random initial condition is significant may last a few hundred days in most aquifers. The constant error in *h(x, t)* in later time is due to the combined effects of the uncertainties in the source/sink and flux boundary: the closer to the flux boundary, the larger the error. The error caused by the uncertain head boundary is limited in a narrow zone near the boundary and remains more or less constant over time. The aquifer system behaves as a low-pass filter which filters out high-frequency noises and keeps low-frequency variations. Temporal scaling of groundwater level fluctuations exists in most part of a low permeable aquifer whose horizontal length is much larger than its thickness caused by the temporal fluctuations of areal source/sink.

Key words: Uncertainty of groundwater levels; Temporal scaling; Random source/sink; Random initial and boundary conditions.~~Uncertainty and scaling of groundwater levels, Random source/sin and initial and boundary conditions.~~

1. Introduction

Groundwater level or hydraulic head (*h*) is the main driving force for water flow and advective contaminant transport in aquifers and thus the most important variable studied in groundwater hydrology and its applications. Knowledge about *h* is critical in dealing with groundwater-related environmental problems, such as over-pumping, subsidence, sea water intrusion, and contamination. One often found that the data about groundwater level is limited or unavailable in a hydrogeological investigation. In such cases the groundwater level distribution and its temporal variation are usually obtained with an analytical or numerical solution to a groundwater flow model.

It is obvious that errors always exit in the groundwater levels calculated or simulated with analytical or numerical solutions~~is obvious that there are some errors exit in S~~~~spatiotemporal variations of groundwater levels calculated or simulated with the analytical or numerical solutions in the realistic case are inherently erroneous~~. The main sources of errors include the simplification or approximation in a conceptual model and the uncertainties in the model parameters. Problems in conceptualization or model structure were dealt with by many researchers (Neuman, 2003;Rojas et al., 2010;Ye et al., 2008;Rojas et al., 2008;Refsgaard et al., 2007;Zeng et al., 2013). The uncertainties in the model parameters (e.g., hydraulic conductivity, recharge rate, evapotranspiration, and river conductance) were investigated based on generalized likelihood uncertainty estimation and Bayesian methods~~, (Beven and Binley, 1992;Vrugt et al., 2003;Neuman et al., 2012)~~ (Nowak et al., 2010;Neuman et

带格式的：字体颜色：自动设置

带格式的：字体颜色：红色

带格式的：字体颜色：红色

带格式的：字体：小四

带格式的：字体：小四，非加粗，字体颜色：自动设置

al., 2012;Rojas et al., 2008;Rojas et al., 2010). The uncertainty in groundwater level has been one of the main research topics in stochastic subsurface hydrology for more than three decades. Most of these studies were focused on the spatial variability of groundwater level due to aquifers' heterogeneity (Dagan, 1989;Gelhar, 1993;Zhang, 2002). Little attention has been given to the uncertainties in groundwater level due to temporal variations of hydrological processes, e.g., recharge, evapotranspiration, discharge to a river, and river stage ~~(Bloomfield and Little, 2010;Zhang and Schilling, 2004;Schilling and Zhang, 2012;Liang and Zhang, 2013a;Zhu et al., 2012).~~ (Bloomfield and Little, 2010;Zhang and Schilling, 2004;Schilling and Zhang, 2012;Liang and Zhang, 2013a;Zhu et al., 2012).

Uncertainties of groundwater level fluctuations have been studied by Zhang and Li (2005, 2006) and most recently by Liang and Zhang (2013a). Based on a linear reservoir model with a white noise or temporally-correlated recharge process, Zhang and Li (2005, 2006) derived the variance and covariance of $h(t)$ by considering only a random source or sink process assuming deterministic initial and boundary conditions. Liang and Zhang (2013a) extended the studies of Zhang and Li (2005, 2006) and carried out non-stationary spectral analysis and Monte Carlo simulations using a linearized Boussinesq equation, and investigated the temporospatial variations of groundwater level. However, the only random process considered by Liang and Zhang (2013a) is the source/sink. Temporal scaling of groundwater levels discovered first by Zhang and Schilling Zhang and Schilling (2004) was verified in several studies (Zhang and Li, 2005, 2006; Bloomfield and Little, 2010; Zhang and

Yang, 2010; Zhu et al., 2012; Schilling and Zhang, 2012). However, we do not know the effect of random boundary conditions on temporal scaling of groundwater levels.

In this study we extended above-mentioned work by considering the groundwater flow in a bounded aquifer described by a linearized Boussinesq equation with a random source/sink as well as random initial and boundary conditions since the latter processes are known with uncertainties. The objectives of this study are 1) to derive analytical solutions for the covariance, variance and spectrum of groundwater level, and 2) to investigate the individual and combined effects of these random processes on uncertainties and scaling of $h(x, t)$. In the following we will first present the formulation and analytical solutions, then discuss the results, and finally draw some conclusions.

2. Formulation and Solutions

Under the Dupuit assumption, the one-dimensional transient groundwater flow in an unconfined aquifer near a river (Fig. 1) can be approximated with the linearized Boussinesq equation (Bear, 1972) with the initial and boundary conditions, i.e.,

$$T\frac{\partial^2 h}{\partial x^2}+W(t)=S_Y\frac{\partial h}{\partial t} \qquad \text{(1a)}$$

$$h(x,t)\big|_{t=0}=H_0(x); \qquad T\frac{\partial h}{\partial x}\bigg|_{x=0}=Q(t); \qquad h(x,t)\big|_{x=L}=H(t) \qquad \text{(1b)}$$

where T [L/T] is the transmissivity, h [L] is the hydraulic head or groundwater level above the bottom of the aquifer which is assumed to be horizontal, $W(t)$ [L/T] is the time-dependent source/sink term representing areal recharge or evapotranspiration, S_Y

is the specific yield, $H_0(x)$ [L] is the initial condition, *Q(t)* [L^2/T] is the time-dependent flux at the left boundary, *H(t)* [L] is the time-dependent water level at the right boundary, *L* [L] is distance from the left to the right boundary, *x* [L] is the coordinate, and *t* [T] is time. In this study the initial head $H_0(x)$ is taken to be a spatially random variable, and the source/sink, *W(t)*, the flux to the left boundary, *Q(t)*, and the head at the right boundary, *H(t)*, are all taken to be temporally random processes and spatially deterministic. The parameters *T* and S_Y are taken to be constant.

The groundwater level, *h(x, t)*, the three random processes, *W(t)*, *Q(t)*, and *H(t)*, and the random variable, $H_0(x)$, are expressed in terms of their respective ensemble means plus small perturbations,

$$h(x,t)=\langle h(x,t)\rangle + h'(x,t) \tag{2a}$$

$$W(t)=\langle W(t)\rangle + W'(t); \qquad Q(t)=\langle Q(t)\rangle + Q'(t) \tag{2b}$$

$$H(t)=\langle H(t)\rangle + H'(t); \qquad H_0(x)=\langle H_0(x)\rangle + H_0'(x) \tag{2c}$$

where < > stands for ensemble average and ' for perturbation. ~~Although the~~The initial condition $H_0(x)$ in (1) can be any function. For the conceptualization of the groundwater flow presented in Fig. 1, the steady-state condition can be reached in ~~an~~this aquifer after a rainfall or during a wet season. Thus the steady-state solution to ~~initial head~~ this model were often adopted as initial condition in previous research (Liang and Zhang, 2012, 2013a, b). Thus, in this study~~, it is appropriate to~~ we set ~~it~~ initial condition $H_0(x)$ to be the steady-state solution to the one-dimensional ~~transient~~ groundwater flow equation, i.e., $H_0(x)=h_0+0.5W_0\left(L^2-x^2\right)/T$, where h_0 [L] is the constant groundwater level at the right boundary and W_0 [L/T] is the spatially constant recharge rate (Liang and Zhang, 2012). Since h_0 is taken to be constant, the

带格式的: 字体: Times New Roman
带格式的: 字体: Times New Roman
带格式的: 字体: 非倾斜
带格式的: 字体: Times New Roman, 小四
带格式的
带格式的: 字体: (中文) 宋体
带格式的: 字体: Times New Roman, 小四
带格式的: 字体颜色: 红色

source of the uncertainty in the initial head $H_0(x)$ is due to random W_0 only. Thus, the mean and perturbation of $H_0(x)$ can be written as, $\langle H_0(x)\rangle = h_0 + 0.5\langle W_0\rangle (L^2 - x^2)/T$ and $H_0'(x) = 0.5W_0'(L^2 - x^2)/T$, respectively. By substituting Eq. (2), $\langle H_0(x)\rangle$, and $H_0'(x)$ into Eq. (1) and taking expectation, one obtains the mean flow equation with the mean initial and boundary conditions as

带格式的：字体颜色：红色

带格式的：字体颜色：红色

$$T\frac{\partial^2\langle h\rangle}{\partial x^2} + \langle W\rangle = S_Y \frac{\partial\langle h\rangle}{\partial t} \tag{3a}$$

$$\langle h(x,0)\rangle = h_0 + \frac{\langle W_0\rangle}{2T}(L^2 - x^2);\quad T\frac{\partial\langle h\rangle}{\partial x}\Big|_{x=0} = \langle Q\rangle;\quad \langle h(L,t)\rangle = \langle H(t)\rangle \tag{3b}$$

Subtracting Eq. (3) from (1) leads to the following perturbation equation with the initial and boundary conditions

$$T\frac{\partial^2 h'}{\partial x^2} + W' = S_Y \frac{\partial h'}{\partial t} \tag{4a}$$

$$h'(x,0) = \frac{W_0'}{2T}(L^2 - x^2);\quad T\frac{\partial h'}{\partial x}\Big|_{x=0} = Q';\quad h'(L,t) = H'(t) \tag{4b}$$

The analytical solution to Eq. (4) can be derived with integral-transform methods (Ozisik, 1968) given by

$$h' = \frac{2}{L}\sum_{n=0}^{\infty} e^{-\beta b_n^2 t}\cos(b_n x)\left[\frac{(-1)^n}{b_n^3 T}W_0' + \beta\int_0^t e^{\beta b_n^2 \xi}\left[\frac{(-1)^n}{T b_n}W'(\xi) - \frac{Q'(\xi)}{T} + H'(\xi)(-1)^n b_n\right]d\xi\right] \tag{5}$$

where $\beta = T/S_Y$, $b_n = (2n+1)\pi/(2L)$. Using Eq. (5), the temporal covariance of the groundwater level fluctuations can be derived as

$$\begin{aligned} C_{hh}(x,t_1;x,t_2) &= E[h'(x,t_1)h'(x,t_2)] \\ &= \frac{4}{L^2}\sum_{m=0}^{\infty}\sum_{n=0}^{\infty} e^{-\beta(b_m^2 t_1 + b_n^2 t_2)}\cos(b_m x)\cos(b_n x)\left[\frac{(-1)^{m+n}}{T^2 b_m^3 b_n^3}\sigma_{W_0}^2 \right.\\ &\left. + \beta^2\int_0^{t_1}\int_0^{t_2} e^{\beta(b_m^2\xi + b_n^2\rho)}\left[\frac{(-1)^{n+m}}{T^2 b_m b_n}C_{WW}(\xi,\rho) + \frac{C_{QQ}(\xi,\rho)}{T^2} + C_{HH}(\xi,\rho)(-1)^{m+n} b_m b_n\right]d\xi d\rho\right] \end{aligned} \tag{6}$$

in which $\sigma^2_{W_0}$ is the variance of W_0, and $C_{WW}(\xi,\rho)$, $C_{QQ}(\xi,\rho)$ and $C_{HH}(\xi,\rho)$ are the temporal auto-covariance of *W(t)*, of *Q(t)*, and *H(t)*, respectively. We assume that *W(t)*, Q*(t)*, and *H(t)* are uncorrelated in order to simplify our analyses. It is shown in Eq. (6) that the head covariance depends on the variance of W_0 and the covariances of *W(t)*, Q*(t)*, and *H(t)* and this equation can be evaluated for any random *W(t)*, Q*(t)*, and *H(t)*. We assume that these processes are white noises as employed in previous studies (Gelhar, 1993;Hantush and Marino, 1994;Liang and Zhang, 2013a). More realistic randomness of these processes will be considered in future studies.

Following *Gelhar* (1993, p.34), we express the spectra of *W(t)*, Q*(t)*, and *H(t)* as $S_{WW}=\sigma^2_W\lambda_W/\pi$, $S_{QQ}=\sigma^2_Q\lambda_Q/\pi$, and $S_{HH}=\sigma^2_H\lambda_H/\pi$, respectively, where σ^2_W, σ^2_Q, and σ^2_H are the variances and λ_W, λ_Q, and λ_H are the correlation time intervals of these three processes, respectively. The corresponding covariance of *W(t)*, *Q(t)* and *H(t)* are $C_{WW}(\xi,\rho)=2\sigma^2_W\lambda_W\delta(\xi-\rho)$, $C_{QQ}(\xi,\rho)=2\sigma^2_Q\lambda_Q\delta(\xi-\rho)$, and $C_{HH}(\xi,\rho)=2\sigma^2_H\lambda_H\delta(\xi-\rho)$. Substituting these covariance into (6) and taking integration, one obtain analytical solution of head covariance

$$C_{hh}(x',t',\tau')=\frac{4\beta L^2}{T^2}\sum_{m=0}^{\infty}\sum_{n=0}^{\infty}\cos(b'_m x')\cos(b'_n x')\left\{e^{-\left[\left(b'^2_m+b'^2_n\right)t'+\left(b'^2_n-b'^2_m\right)\frac{\tau'}{2}\right]}\frac{L^2(-1)^{m+n}\sigma^2_{W_0}}{\beta b'^3_m b'^3_n}\right.$$
$$\left.+2\frac{\left(e^{-b'^2_m\tau'}-e^{-2b'^2_m t'}\right)}{\left(b'^2_m+b'^2_n\right)}\left[\frac{(-1)^{m+n}\sigma^2_W\lambda_W}{b'_m b'_n}+\frac{\sigma^2_Q\lambda_Q}{L^2}+\frac{(-1)^{m+n}b'_m b'_n T^2\sigma^2_H\lambda_H}{L^4}\right]\right\} \tag{7}$$

where $\tau'=t'_2-t'_1$ and $t'=(t'_2+t'_1)/2$. The analytical solution for the head variance can be obtain by setting $\tau'=0$

$$\sigma_h^2(x',t') = \frac{4\beta L^2}{T^2}\sum_{m=0}^{\infty}\sum_{n=0}^{\infty}\cos(b'_m x')\cos(b'_n x')\left\{ e^{-\left(b'^2_m + b'^2_n\right)t'}\frac{L^2}{\beta}\frac{(-1)^{m+n}\sigma_{W_0}^2}{b'^3_m b'^3_n} + 2\frac{1-e^{-2b'^2_m t'}}{\left(b'^2_m + b'^2_n\right)}\left[\frac{(-1)^{m+n}\sigma_W^2\lambda_W}{b'_m b'_n} + \frac{\sigma_Q^2\lambda_Q}{L^2} + \frac{(-1)^{m+n}b'_m b'_n T^2\sigma_H^2\lambda_H}{L^4}\right]\right\} \tag{8}$$

where

$$t' = \frac{t}{t_c};\quad x' = \frac{x}{L};\quad t_c = \frac{L^2}{\beta};\quad b'_n = \frac{(2n+1)\pi}{2}$$

in which $t_c (= S_Y L^2/(KM))$ [1/T] is a characteristic timescale (Gelhar, 1993) where the transmissivity (*T*) is replaced by the product of the hydraulic conductivity (*K*) and the average saturated thickness (*M*) of the aquifer. The characteristic timescale (t_c) is an important parameter and its value for most shallow aquifers is usually larger than 100 day since the horizontal extent of a shallow aquifer is usually much larger than its thickness. For instance, the value of t_c is 250 days for a sandy aquifer with L=100m, M =10m, K=1m/day, and S_Y=0.25.

The spectral density of *h(x, t)* can't be derived by ordinary Fourier transform since the head covariance and variance depend on time *t'* and thus *h(x, t)* are temporally non-stationary as shown in Eqs. (7) and (8). Priestley (1981) defined the spectral density of non-stationary processes (Wigner spectrum) as the Fourier transform of time-dependent auto-covariance with fixed reference time *t* and derived time-dependent spectral density. In order to obtain the spectrum of *h(x, t)*, we applied Priestley's method and obtained the time-dependent spectral density (Priestley, 1981; Zhang and Li, 2005;Liang and Zhang, 2013a), i.e.,

$$\begin{aligned} S_{hh}(x,t,\omega) &= \frac{1}{2\pi}\int_{-\infty}^{\infty} C_{hh}(x,t,\tau)e^{-i\omega\tau}d\tau \\ &= \sum_{m=0}^{\infty}\sum_{n=0}^{\infty}\cos(b_m x)\cos(b_n x)\frac{2t_c\left(b_n^2 - b_m^2\right)e^{-\beta\left(b_m^2+b_n^2\right)t}}{\beta^2\left(b_n^2-b_m^2\right)^2/4+\omega^2}\frac{(-1)^{m+n}\sigma_{W_0}^2}{\pi T^2 b_m^3 b_n^3} + \\ &\sum_{m=0}^{\infty}\sum_{n=0}^{\infty}\cos(b_m x)\cos(b_n x)\frac{8\beta b_m^2}{t_c\left(b_m^2+b_n^2\right)}\frac{1}{\beta^2 b_m^4+\omega^2}\left[\frac{(-1)^{m+n}S_{WW}}{T^2 b_m b_n} + \frac{S_{QQ}}{T^2} + (-1)^{m+n}b_m b_n S_{HH}\right] \end{aligned} \tag{9}$$

where ω is angular frequency and $\omega = 2\pi f$, f is frequency, and $i=\sqrt{-1}$. It is seen in Eq. (9) that the spectrum S_{hh} is dependent on not only frequency and locations but also time t. The time-dependent term (i.e., first term) in Eq. (9) is caused by the random initial condition and is proportional to $e^{-\beta\left(b_m^2+b_n^2\right)t}$ which decays quickly with t. We evaluated the first term in the Eq. (9) by setting t=0 and found that it is much smaller than the second term in Eq. (9). We thus ignored the first term and evaluated the spectrum using the approximation,

$$S_{hh}(x',\omega)=\sum_{m=0}^{\infty}\sum_{n=0}^{\infty}\frac{8\beta b'^2_m\cos(b'_m x')\cos(b'_n x')}{t_c\left(b'^2_m+b'^2_n\right)\left(\beta^2 b'^4_m/L^4+\omega^2\right)}\left[\frac{(-1)^{m+n}S_{WW}L^2}{T^2 b'_m b'_n}+\frac{S_{QQ}}{T^2}+\frac{(-1)^{m+n}b'_m b'_n S_{HH}}{L^2}\right] \quad (10)$$

3. Results and Discussion

3.1 Variance of groundwater levels

The general expression of the head variance in Eq. (8) depends on the variances of the four random processes, $\sigma^2_{W_0}$, σ^2_W, σ^2_Q, and σ^2_H. In the following we will study their individual and combined effects on the head variation and focus our attention only on the variance of $h(x, t)$. The dimensionless standard deviation of $h(x, t)$, σ'_h , or the square root of the dimensionless variance (σ'^2_h) as a function of the dimensionless time (t') were evaluated and presented in the left column of Fig. 2 at fixed dimensionless locations (x'). The σ'_h as a function of x' was evaluated and presented in the right column of Fig. 2 at fixed t'.

We first evaluate the effect of the random initial condition due to the random term, W_0, by setting ~~the variances of $W(t)$, $Q(t)$ and $H(t)$ to be zero, i.e.,~~ $\sigma^2_W=\sigma^2_Q=\sigma^2_H=0$. In this case the dimensionless variance in Eq. (8) reduces to

带格式的: 字体: 倾斜
带格式的: 非升高量 / 降低量
带格式的: 非升高量 / 降低量
带格式的: 字体: 倾斜, 非升高量 / 降低量
带格式的: 非升高量 / 降低量
带格式的: 非升高量 / 降低量
带格式的: 字体: 倾斜

$$\sigma'^2_h(x',t') = \sum_{m=0}^{\infty}\sum_{n=0}^{\infty} \frac{(-1)^{m+n}}{b'^3_m\, b'^3_n}\cos(b'_m\, x')\cos(b'_n\, x')e^{-\left(b'^2_m+b'^2_n\right)t'} \qquad (11)$$

where $\sigma'^2_h = \sigma^2_h T^2/(4L^4\sigma^2_{W_0})$. ~~The~~ The changes of the ~~dimensionless standard deviation of *h(x, t)*,~~ σ'_h ~~,~~ with *x'* and *t'* were presented in Fig 2a and 2b, respectively.~~or the square root of the dimensionless variance (σ'^2_h) in Eq. (11) as a function of the dimensionless time (*t'*) was evaluated and presented in Fig.~~ 2a. ~~1a at five dimensionless locations, *x'* = 0, 0.2, 0.4, 0.6, and 0.8.~~ It is shown in Fig. ~~1a~~ 2a that for a fixed location the ~~standard deviation~~ σ'_h is at its maximum at *t'*=0 and decreases with time gradually to a negligible number at *t'*=1.0. This means that the error in *h(x, t)* predicted by an analytical or numerical solution due to the uncertain initial condition is significant at early time, especially near a flux boundary. The time duration during which the effect of the uncertain initial condition is significant depends on the value of the characteristic timescale (t_c) since $t'=t/t_c$. In the most aquifers this duration may last many days. In the typical aquifer studied ~~with *L*=100m, *M* =10m, *K*=1m/day, and *S_y*=0.25~~ the effect of the uncertainty in initial condition on *h(x, t)* is significant during first 250 days (*t'*=1.0). This duration should be relatively short, however, in a more permeable aquifer whose horizontal extent (*L*) is relatively smaller than its thickness (*M*). ~~The dimensionless standard deviation (σ'_h) based on Eq. (11) as a function of the dimensionless location (*x'*) was presented in Fig. 1b~~ 2b ~~for five dimensionless times, *t'* = 0.0, 0.2, 0.4, 0.6, and 0.8.~~ It is seen in Fig. ~~1b~~ 2b that for a fixed time, the σ'_h is the largest at the left flux boundary (*x'*=~~-~~0.0) and becomes zero at the right constant head boundary (*x'*=1.0)

带格式的: 字体: 倾斜

带格式的: 字体: 倾斜

since the right boundary is ~~known~~deterministic. This means that the error in *h(x, t)* predicted by an analytical or numerical solution due to the uncertain initial condition is significant almost everywhere in the aquifer: the further away from a constant head boundary~~ or the closer to a flux boundary~~, the larger the error.

We then consider the uncertainty in the areal source/sink term (*W*) by setting $\sigma_{W_0}^2 = \sigma_Q^2 = \sigma_H^2 = 0$. In this case the dimensionless variance in Eq. (8) reduces to

$$\sigma'^2_h(x',t') = 2\sum_{m=0}^{\infty}\sum_{n=0}^{\infty}\cos(b'_m x')\cos(b'_n x')\frac{(1-e^{-2b'^2_m t'})(-1)^{m+n}}{(b'^2_m + b'^2_n)b'_m b'_n} \qquad (12)$$

where $\sigma'^2_h = \sigma_h^2 TS_Y/(4L^2\sigma_W^2\lambda_W)$. The changes of the σ'_h with *x'* and *t'* were presented in Fig 2c and 2d, respectively.~~The dimensionless standard deviation (σ'_h) based σ'^2_h in Eq. (12) as a function of the dimensionless time (*t'*) for the same five locations, *x'*=0.0, 0.2, 0.4, 0.6, and 0.8, was presented in Fig. 1c2c.~~ It is noticed in Fig. 2c that at a fixed location, the σ'_h is zero initially, gradually increases as time goes, and approaches a constant limit at later time. This means that the error in *h(x, t)* due to an source/sink is at its minimum at early time and increases with time to approach a constant limit at later time: the closer to the left flux boundary, the larger the limit. ~~The dimensionless standard deviation (σ'_h) versus the dimensionless location (x') for the dimensionless time, *t'*=0.0, 0.2, 0.4, 0.6, and 0.8, is presented in Fig. 1d2d.~~ For a fixed time the σ'_h decreases smoothly from the left to the right boundary (Fig. 2d). The error in *h(x, t)* due to the uncertainty in the source/sink is significant almost everywhere in the aquifer: the further away from the constant head boundary~~ or the closer to a flux boundary~~, the larger the error, similar to the previous case with the random initial condition (Fig. ~~1b~~2b).

Thirdly, we investigate the effect of the left random flux boundary by setting $\sigma^2_{W_0} = \sigma^2_W = \sigma^2_H = 0$ in Eq. (8). In this case the dimensionless head variance is given by

$$\sigma'^2_h(x',t') = 2\sum_{m=0}^{\infty}\sum_{n=0}^{\infty}\cos(b'_m x')\cos(b'_n x')\frac{1-e^{-2b'^2_m t'}}{b'^2_m + b'^2_n} \qquad (13)$$

where $\sigma'^2_h = \sigma^2_h T S_Y/(4\sigma^2_Q \lambda_Q)$. The changes of the σ'_h with *x'* and *t'* were presented in Fig 2e and 2f, respectively.~~The dimensionless standard deviation (σ'_h) based on Eq. (13) as a function of the dimensionless time (t') is plotted in Fig. 1e~~ 2e ~~for *x'*=0.0, 0.2, 0.4, 0.6 and 0.8. Similar to the case of the random source/sink in Fig. 1c~~2c~~, a~~At any location the σ'_h in Fig. ~~1e~~ 2e or the error in *h(x, t)* due to an uncertain flux boundary is at its minimum at early time and increases quickly with time to approach a constant limit: the closer to the left flux boundary, the larger the limit. ~~The dimensionless deviation (σ'_h) as a function of the dimensionless location (x') is plotted in Fig. 1f~~ 2f ~~for *t'*=0.01, 0.1, and 1.0.~~ At any time the σ'_h in ~~this case~~ Fig. 2f or the error in the head due to the uncertain flux boundary is at its maximum at the left boundary but decreases quickly away from the boundary to become insignificant for *x'*>0.8.

Fourthly, we investigated the effect of the random head boundary by setting $\sigma^2_{W_0} = \sigma^2_W = \sigma^2_Q = 0$ in Eq. (8). The dimensionless head variance in this case is given by

$$\sigma'^2_h(x',t') = 2\sum_{m=0}^{\infty}\sum_{n=0}^{\infty}\cos(b'_m x')\cos(b'_n x')\frac{(-1)^{m+n} b'_m b'_n \left(1-e^{-2b'^2_m t'}\right)}{\left(b'^2_m + b'^2_n\right)} \qquad (14)$$

where $\sigma'^2_h = \sigma^2_h L^2 S_Y/(4T\sigma^2_H \lambda_H)$. The changes of this σ'_h with *x'* and *t'* were presented in Fig 2g and 2h, respectively.~~The dimensionless standard deviation (σ'_h) based on Eq. (14) as a function of the dimensionless time (t') is provided in Fig. 1g~~2g ~~for x'=0.0, 0.2, 0.4, 0.6, and 0.8.~~ It seen in Fig. 2g that ~~Similar to the case of the random flux boundary (Fig. 1e~~2e~~), a~~at any location the σ'_h or the error in *h(x, t)* due to the random head boundary increases with time quickly to approach a constant limit: the closer to the uncertain head boundary, the larger the error. The spatial variation of σ'_h can be clearly observed in Fig. ~~1h~~ 2h for ~~t'=0.01, 0.1, and 1.0~~fixed *t'*. At any time σ'_h is at its maximum at the right boundary (*x'*=1) where the head is uncertain, decreases quickly away from the boundary. The error in *h(x, t)* due to the uncertain head boundary is limited in a narrow zone near the boundary (*x'*>0.8) (Fig. ~~1h~~2h).

Finally, we consider the combined effects of the uncertainties from all four sources, i.e., the initial condition, sources, and flux and head boundaries. The head variance in Eq. (8) is written in the dimensionless form as

$$\sigma'^2_h(x',t') = \sum_{m=0}^{\infty}\sum_{n=0}^{\infty}\cos(b'_m x')\cos(b'_n x')\left\{ e^{-\left(b'^2_m + b'^2_n\right)t'} \frac{(-1)^{m+n}\sigma'^2_{W_0}}{b'^3_m b'^3_n} + 2\frac{1-e^{-2b'^2_m t'}}{\left(b'^2_m + b'^2_n\right)}\left[\frac{(-1)^{m+n}}{b'_m b'_n} + \sigma'^2_Q + (-1)^{m+n} b'_m b'_n \sigma'^2_H\right]\right\} \tag{15}$$

where

$$\sigma'^2_h = \frac{\sigma^2_h T S_Y}{4L^2\sigma^2_W \lambda_W};\quad \sigma'^2_{W_0} = \frac{L^2 S_Y \sigma^2_{W_0}}{T\sigma^2_W \lambda_W};\quad \sigma'^2_Q = \frac{\sigma^2_Q \lambda_Q}{L^2\sigma^2_W \lambda_W};\quad \sigma'^2_H = \frac{T^2\sigma^2_H \lambda_H}{L^4\sigma^2_W \lambda_W}$$

带格式的: 字体: 非倾斜

带格式的: 字体: 非倾斜

The dimensionless variances, $\sigma'^2_{W_0}$, σ'^2_Q and σ'^2_H, need to be specified in order to evaluate the dimensionless $\sigma'^2_h(x',t')$ in Eq. (15). For the typical aquifer mentioned above with L=100m, T=10 m^2/day (or K=1m/day and M=10m) and S_Y=0.25, we set $\sigma^2_{W_0}/(\sigma^2_W\lambda_W)=10^{-1}$, $\sigma^2_Q\lambda_Q/(\sigma^2_W\lambda_W)=10^3$, $\sigma^2_H\lambda_H/(\sigma^2_W\lambda_W)=10^4$ and obtain $\sigma'^2_{W_0}=25$, $\sigma'^2_Q=0.1$ and $\sigma'^2_H=0.01$.

The changes of this σ'_h with x' and t' were presented in Fig 2i and 2j, respectively.~~The dimensionless standard deviation (σ'_h) based on Eq. (15) as a function of the dimensionless time (t') is presented in Fig. 2a~~ 2i ~~for x'=0.0, 0.2, 0.4, 0.6, and 0.8.~~ It is observed in Fig. ~~2a~~ 2i that at any location the σ'_h is at its maximum due to the uncertainty in the initial condition, gradually decreases as time goes, and approaches a constant limit at later time (t'>0.6) which is due to the combined effects of the uncertain source/sink and flux and head boundaries. This means that the error in the head in early time is significant if the initial condition is uncertain and reduces as time goes to reach a constant limit~~ or error in later time~~. The error in head in later time is determined by the uncertainties in the source/sink, flux and head boundaries. ~~The spatial variation of the dimensionless standard deviation (σ'_h) for this case is provided in Fig. 2b~~ 2j ~~for t'=0.01, 0.2, 0.4, 0.6, and 0.8.~~ It can be observed in Fig. 2j that σ'_h is relatively larger near both boundaries. The values of σ'_h at the two boundaries are equivalent (~1.3) at early time, say t'=0.01 (the top curve in Fig. ~~2b~~2j) and it reduces slowly away from the flux boundary but quickly away from the head boundary. As time progresses, the σ'_h near the head boundary stays more or less the same but reduces significantly in most part of the aquifer. This means that in early time the error in *h(x, t)* in most part of the aquifer is mainly caused by the initial condition and at later time it is due to the combined effects of the uncertain areal source/sink and flux boundary. The effect of the uncertain head boundary on *h(x, t)* doesn't change with time significantly but is limited in a narrow zone near the boundary.

3.2 Spectrum of groundwater levels

We first evaluated S_{hh} in Eq. (10) due to the effect of the white noise flux boundary only by setting $S_{QQ} \neq 0$, $S_{WW} = 0$, and $S_{HH} = 0$. The dimensionless spectrum S_{hh}/S_{QQ} as a function of the frequency (*f*) was evaluated and presented in the log-log plot (Fig. 3a-3c) for three values of t_c (40, 400, and 4,000 days) since the value of t_c is 250 days for a sandy aquifer~~ with L=100m, M =10m, K=1m/day, and S_y=0.25~~ as we mentioned above and at the six locations (*x'* = 0.0, 0.2, 0.4, 0.6, 0.8, and 0.9). The spectrum S_{hh}/S_{QQ} in Fig. 3a is more or less horizontal (i.e., white noise) at low frequencies and decrease gradually as *f* increases, indicating that an aquifer acts as a low-bass filter that filter signals at high frequencies and keep signals at low frequencies. The aquifer has significantly dampened the fluctuations of the groundwater level. The spectrum varies with the location *x'*: the smaller the value of *x'* or the closer to the left flux boundary (*x'*=0), the larger the spectrum (Fig. 3a-3c). All spectra in Fig. 3a are not a straight line in the log-log plot, meaning that the temporal scaling of *h(x, t)* doesn't exist in the range of f =10^{-3}~10^{0} when t_c=40 days. As t_c increases to 400 and 4000 days, however, the spectrum at *x'*=0 become a straight line (the top curve in Fig. 3b and 3c) or has a power-law relation with *f*, i.e.,

$S_{hh}/S_{QQ} \propto 1/f$, since its slope is approximately one. The fluctuations of *h(0, t)* is a pink noise due to the white noise fluctuations flux boundary when the characteristic timescale (t_c) is large which means that the aquifer is relatively less permeable and/or has a much larger horizontal length than its thickness.

Secondly, the spectrum S_{hh}/S_{HH} due to the sole effect of the random head boundary was evaluated by setting $S_{HH} \neq 0$, $S_{WW} = 0$, and $S_{QQ} = 0$ in Eq. (10) for the same three values of t_c and six locations and presented in Fig. 3d-3f as a function of *f*. It is shown that similar to Fig. 3a-3c, the spectrum decreases as *f* increases but different from Fig. 3a-3c, the spectrum is larger at *x'*=0.9 near the right boundary (the top curves in Fig. 3d-3f) than that *x'*=0.0 (the bottom curves). Furthermore, none of the spectra are a straight line in the log-log plot, indicating that the temporal scaling of groundwater level fluctuations doesn't exist in the case of the white noise head boundary.

Thirdly, the spectrum S_{hh}/S_{WW} due the effect of the white noise recharge only was evaluated by setting $S_{WW} \neq 0$, $S_{QQ} = 0$, and $S_{HH} = 0$ in Eq. (10) for the same values of t_c and *x'* and presented in Fig. 3g-3i as a function of *f*. It is shown that when t_c=40 day the spectrum in Fig. 3g is horizontal at low frequencies and become a straight line at high frequencies: the closer to the right head boundary, the later it approaches a straight line (Fig. 3h). As t_c increases to 400 and 4000 days, the slope of the spectrum at all locations except at *x'*=0.9 approaches to a straight line with a slope of 2 (Fig. 3h and 3i), indicating a temporal scaling of *h(x, t)*. The fluctuations of groundwater level is a Brownian motion, i.e., $S \propto 1/f^2$, when $t_c \geq 4000$ day or in a relatively less permeable and/or has a much larger horizontal length than its thickness.

Finally, the head spectrum due to the combined effect of all three random sources (the white noise recharge, and flux and head boundaries) was evaluated, i.e., $S_{WW} \neq 0$, $S_{QQ} \neq 0$, and $S_{HH} \neq 0$ in Eq. (10). The spectrum of S_{hh}/S_{WW} as a function of *f* was presented in Fig. ~~-4~~3j-3l for the same values of t_c and *x'* where $S_{QQ}/S_{WW} = 1000$ and $S_{HH}/S_{WW} = 10000$ which are same with the values using in previous section. It is noticed that the general patterns of S_{hh}/S_{WW} in the combined case ~~(Fig. 4)~~ is similar to the case under the random source/sink only (Fig. 3g-3i) except at *x'*=0.0 and 0.9 (the dashed and dotted curves in Fig. ~~4a~~3j, respectively) due to the strong effects of the boundary conditions at these two locations. At t_c=4000 day, the spectra at all locations except *x'*=0.0 (Fig. ~~4c~~3l) are similar to those in Fig. 3i, indicating the dominating effect of the random areal source/sink. The spectrum at *x'*=0 in this case is also a straight line (the dashed curve in Fig. ~~4c~~3l) but with a different slope due to the effect of the random flux boundary which is similar to the top straight line in Fig. 3c. Above results provide a theoretical explanation as why temporal scaling exists in the observed groundwater level fluctuations (Zhang and Schilling, 2004;Bloomfield and Little, 2010;Zhu et al., 2012). We thus conclude that temporal scaling of *h(x, t)* may indeed exist in real aquifers due to the strong effect of the areal source/sink.

~~It is noted that the~~

4. Conclusions

In this study the effects of random source/sink, and initial and boundary conditions on the uncertainty and temporal scaling of the groundwater level, *h(x, t)* were investigated. The analytical solutions for the variance, covariance and spectrum of *h(x, t)* in an unconfined aquifer described by a linearized Boussinesq equation with white noise source/sink, and initial and boundary conditions were derived. The standard deviations of *h(x, t)* for various cases were evaluated. Based on the results, the following conclusions can be drawn.

1. The error in *h(x, t)* due to a random initial condition is significant at early time, especially near a flux boundary. The duration during which the effect is significant may last a few hundred days in most aquifers;

2. The error in *h(x, t)* due to a random areal source/sink is significant in most part of an aquifer: the closer to a flux boundary, the larger the error;

3. The errors in *h(x, t)* due to random flux and head boundaries are significant near the boundaries: the closer to the boundaries, the larger the errors. The random flux boundary may affect the head over a larger region near the boundary than the random head boundary;

4. In the typical sandy aquifer studied (with the length of aquifer at the direction of water flow L=100m, the average saturated thickness M =10m, hydraulic conductivity K=1m/day, and specific yield S_Y=0.25) the error in *h(x, t)* in early time is mainly caused by an uncertain initial condition and the error reduces as time goes to reach a constant error in later time. The constant error in *h(x, t)* is mainly due to the combined effects of uncertain source/sink and boundaries;

带格式的：缩进：左侧：0 厘米，首行缩进：1.77 字符

带格式的：字体：小四

带格式的：字体：小四

带格式的：字体：小四

5. The aquifer system behaves as a low-pass filter which filter the short-term (~~low~~ high frequencies) fluctuations and keep the long-term (low frequencies) fluctuations;

6. Temporal scaling of groundwater level fluctuations may indeed exist in most part of a low permeable aquifer whose horizontal length is much larger than its thickness caused by the temporal fluctuations of areal source/sink.

Finally, it is pointed out that the analyses carried out in this study is under the assumptions that the processes, *W(t)*, Q*(t)*, and *H(t)* are uncorrelated white noises. In reality, they may be correlated and spatially varied. We plan to relax those constrains and study more realistic cases in the near future. It is also noted that the analytical solutions for head variances derived in this study provide a way to identify and quantify the uncertainty. The spectrum relationship obtained among the head, recharge and boundary conditions can help one to improve spectrum analysis for a groundwater level time series and removed the effects of the boundary conditions.

Acknowledgment

This study was partially supported with the research grants from the National Nature Science Foundation of China (NSFC-41272260; NSFC-41330314; NSFC-41302180), the Natural Science Foundation of Jiangsu Province (SBK201341336) and from the National Key project “Water Pollution Control in the Huai River Basin” of China (2012ZX07204-001, 2012ZX07204-003).

References

Bear, J.: Dynamics of fluids in porous media, Environmental science series (New York, 1972-), American Elsevier Pub. Co., New York,, xvii, 764 p. pp., 1972.

Beven, K., and Binley, A.: The Future of Distributed Models - Model Calibration and Uncertainty Prediction, Hydrol Process, 6, 279-298, 1992.

Bloomfield, J. P., and Little, M. A.: Robust evidence for random fractal scaling of groundwater levels in unconfined aquifers, J Hydrol, 393, 362-369, DOI 10.1016/j.jhydrol.2010.08.031, 2010.

Dagan, G.: Flow and transport in porous formations, Springer-Verlag, Berlin ; New York, xvii, 465 p. pp., 1989.

Gelhar, L. W.: Stochastic subsurface hydrology, Prentice-Hall, Englewood Cliffs, N.J., x, 390 p. pp., 1993.

Hantush, M. M., and Marino, M. A.: One-Dimensional Stochastic-Analysis in Leaky Aquifers Subject to Random Leakage, Water Resour Res, 30, 549-558, Doi 10.1029/93wr02887, 1994.

Liang, X. Y., and Zhang, Y. K.: A new analytical method for groundwater recharge and discharge estimation, J Hydrol, 450, 17-24, DOI 10.1016/j.jhydrol.2012.05.036, 2012.

Liang, X. Y., and Zhang, Y. K.: Temporal and spatial variation and scaling of groundwater levels in a bounded unconfined aquifer, J Hydrol, 479, 139-145, DOI 10.1016/j.jhydrol.2012.11.044, 2013a.

Liang, X. Y., and Zhang, Y. K.: Analytic solutions to transient groundwater flow under time-dependent sources in a heterogeneous aquifer bounded by fluctuating river stage, Adv Water Resour, 58, 1-9, DOI 10.1016/j.advwatres.2013.03.010, 2013b.

~~Liang, X. Y., and Zhang, Y. K.: A new analytical method for groundwater recharge and discharge estimation, J Hydrol, 450, 17-24, DOI 10.1016/j.jhydrol.2012.05.036, 2012.~~

~~Liang, X. Y., and Zhang, Y. K.: Temporal and spatial variation and scaling of groundwater levels in a bounded unconfined aquifer, J Hydrol, 479, 139-145, DOI 10.1016/j.jhydrol.2012.11.044, 2013.~~

Neuman, S. P.: Maximum likelihood Bayesian averaging of uncertain model predictions, Stoch Env Res Risk A, 17, 291-305, 10.1007/s00477-003-0151-7, 2003.

Neuman, S. P., Xue, L., Ye, M., and Lu, D.: Bayesian analysis of data-worth considering model and parameter uncertainties, Advances in Water Resources, 36, 75-85, 10.1016/j.advwatres.2011.02.007, 2012.

Nowak, W., de Barros, F. P. J., and Rubin, Y.: Bayesian geostatistical design: Task-driven optimal site investigation when the geostatistical model is uncertain, Water Resour Res, 46, Artn W03535 Doi 10.1029/2009wr008312, 2010.

带格式的: 缩进: 悬挂缩进: 2.12 字符, 左 0.01 字符, 首行缩进: -2.12 字符

Priestley, M. B.: Spectral Analysis and Time Series, Academic Press, San Diego, 1981.

Refsgaard, J. C., van der Sluijs, J. P., Hojberg, A. L., and Vanrolleghem, P. A.: Uncertainty in the environmental modelling process - A framework and guidance, Environmental Modelling & Software, 22, 1543-1556, 10.1016/j.envsoft.2007.02.004, 2007.

Rojas, R., Feyen, L., and Dassargues, A.: Conceptual model uncertainty in groundwater modeling: Combining generalized likelihood uncertainty estimation and Bayesian model averaging, Water Resources Research, 44, 10.1029/2008wr006908, 2008.

Rojas, R., Feyen, L., Batelaan, O., and Dassargues, A.: On the value of conditioning data to reduce conceptual model uncertainty in groundwater modeling, Water Resources Research, 46, 20, 10.1029/2009wr008822, 2010.

Schilling, K. E., and Zhang, Y. K.: Temporal Scaling of Groundwater Level Fluctuations Near a Stream, Ground Water, 50, 59-67, DOI 10.1111/j.1745-6584.2011.00804.x, 2012.

Vrugt, J. A., Gupta, H. V., Bouten, W., and Sorooshian, S.: A Shuffled Complex Evolution Metropolis algorithm for optimization and uncertainty assessment of hydrologic model parameters, Water Resources Research, 39, 10.1029/2002wr001642, 2003.

Ye, M., Meyer, P. D., and Neuman, S. P.: On model selection criteria in multimodel analysis, Water Resources Research, 44, 10.1029/2008wr006803, 2008.

Zeng, X. K., Wang, D., Wu, J. C., and Chen, X.: Reliability Analysis of the Groundwater Conceptual Model, Human and Ecological Risk Assessment, 19, 515-525, 10.1080/10807039.2012.713822, 2013.

Zhang, D.: Stochastic methods for flow in porous media : coping with uncertainties, Academic, San Diego, Calif. London, xiv, 350 p. pp., 2002.

Zhang, Y. K., and Schilling, K.: Temporal scaling of hydraulic head and river base flow and its implication for groundwater recharge, Water Resour Res, 40, -, Artn W03504
Doi 10.1029/2003wr002094, 2004.

Zhang, Y. K., and Li, Z. W.: Temporal scaling of hydraulic head fluctuations: Nonstationary spectral analyses and numerical simulations, Water Resources Research, 41, 10.1029/2004wr003797, 2005.

Zhang, Y. K., and Li, Z. W.: Effect of temporally correlated recharge on fluctuations of groundwater levels, Water Resources Research, 42, 10.1029/2005wr004828, 2006.

Zhang, Y. K., and Yang, X. Y.: Effects of variations of river stage and hydraulic conductivity on temporal scaling of groundwater levels: numerical simulations, Stoch Env Res Risk A, 24, 1043-1052, DOI 10.1007/s00477-010-0437-5, 2010.

Zhu, J. T., Young, M. H., and Osterberg, J.: Impacts of riparian zone plant water use on temporal scaling of groundwater systems, Hydrol Process, 26, 1352-1360, Doi 10.1002/Hyp.8241, 2012.

Figure captions

Figure 1 A schematic of the unconfined aquifer studied where $W(t)$ is the random time-dependent source/sink, $H_0(x)$ is the random initial condition, $Q(t)$ is the random time-dependent flux at the left boundary, $H(t)$ is the random time-dependent water level at the right boundary, L is distance from the left to the right boundary, and $h(x, t)$ is the random groundwater level in the aquifer.

Figure 2 The graphs on the left column are the standard deviation (σ'_h) of groundwater level ($h(x, t)$) versus the dimensionless time (t') at the dimensionless locations x'=0.0, 0.2, 0.4, 0.6, and 0.8. The graphs on the right column are σ'_h versus x' for the different t': b) and d) are for t'= 0.0, 0.2, 0.4, 0.6 and 0.8, f) and h) are for t'=0.01, 0.1, and 1.0, and j) is for t'=0.01, 0.2, 0.4, 0.6 and 0.8. Also, a) and b) are based on Eq.(11) where $\sigma_W^2 = \sigma_Q^2 = \sigma_H^2 = 0$; c) and d) are based on Eq. (12) where $\sigma_{W_0}^2 = \sigma_Q^2 = \sigma_H^2 = 0$; e) and f) are based on Eq. (13) where $\sigma_{W_0}^2 = \sigma_W^2 = \sigma_H^2 = 0$; g) and h) are based on Eq. (14) where $\sigma_{W_0}^2 = \sigma_W^2 = \sigma_Q^2 = 0$; i) and j) are based on Eq.(15) where $\sigma_{W_0}^2 \neq \sigma_W^2 \neq \sigma_Q^2 \neq \sigma_H^2 \neq 0$.

Figure 3 The dimensionless power spectrum versus frequency (f) at the dimensionless locations x'=0.0, 0.2, 0.4, 0.6, 0.8, and 0.9. The graphs on the left column are for t_c = 40 day, the graphs on the middle column are for t_c = 400 day, and the graphs on the right column are for t_c = 4000 day. The graphs on the first row are the dimensionless spectrum S_{hh}/S_{QQ} when $S_{WW}=0$, $S_{HH}=0$, and $S_{QQ}\neq 0$ in Eq. (10), the graphs on the second row is S_{hh}/S_{HH} when $S_{WW}=0$, $S_{QQ}=0$, and $S_{HH}\neq 0$, the graphs on the third row are S_{hh}/S_{WW} when $S_{QQ}=0$, $S_{HH}=0$, and $S_{WW}\neq 0$, and the graphs on the bottom row is S_{hh}/S_{WW} when $S_{QQ}\neq 0$, $S_{HH}\neq 0$, and $S_{WW}\neq 0$.

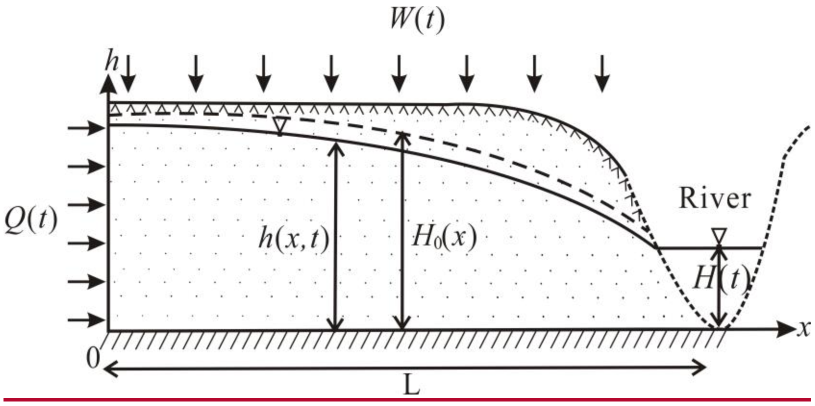

Figure 1

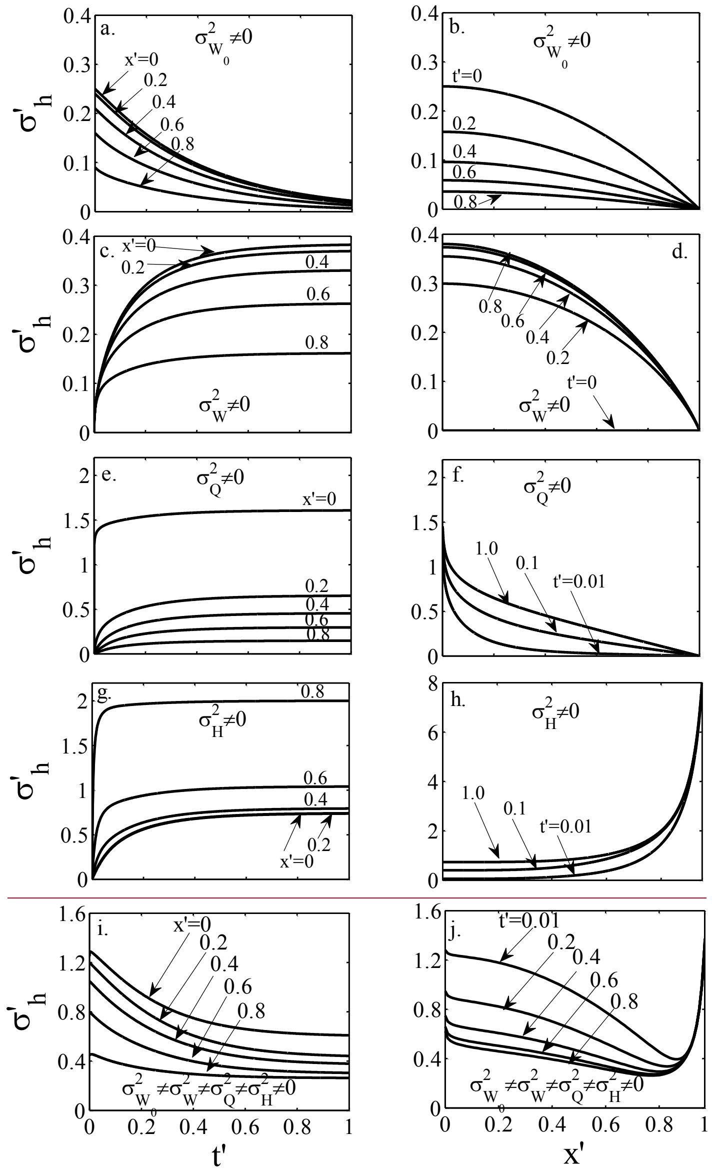

a.
$\sigma^2_{W_0}\neq0$
x'=0
0.2
0.4
0.6
0.8
b.
$\sigma^2_{W_0}\neq0$
t'=0
0.2
0.4
0.6
0.8
c.
x'=0
0.2
0.4
0.6
0.8
$\sigma^2_W\neq0$
d.
0.8
0.6
0.4
0.2
t'=0
$\sigma^2_W\neq0$
e.
$\sigma^2_Q\neq0$
x'=0
0.2
0.4
0.6
0.8
f.
$\sigma^2_Q\neq0$
1.0
0.1
t'=0.01
g.
0.8
$\sigma^2_H\neq0$
0.6
0.4
0.2
x'=0
h.
$\sigma^2_H\neq0$
1.0
0.1
t'=0.01
i.
x'=0
0.2
0.4
0.6
0.8
$\sigma^2_{W_0}\neq\sigma^2_W\neq\sigma^2_Q\neq\sigma^2_H\neq0$
j.
t'=0.01
0.2
0.4
0.6
0.8
$\sigma^2_{W_0}\neq\sigma^2_W\neq\sigma^2_Q\neq\sigma^2_H\neq0$
σ'_h
t'
x'

Figure 2

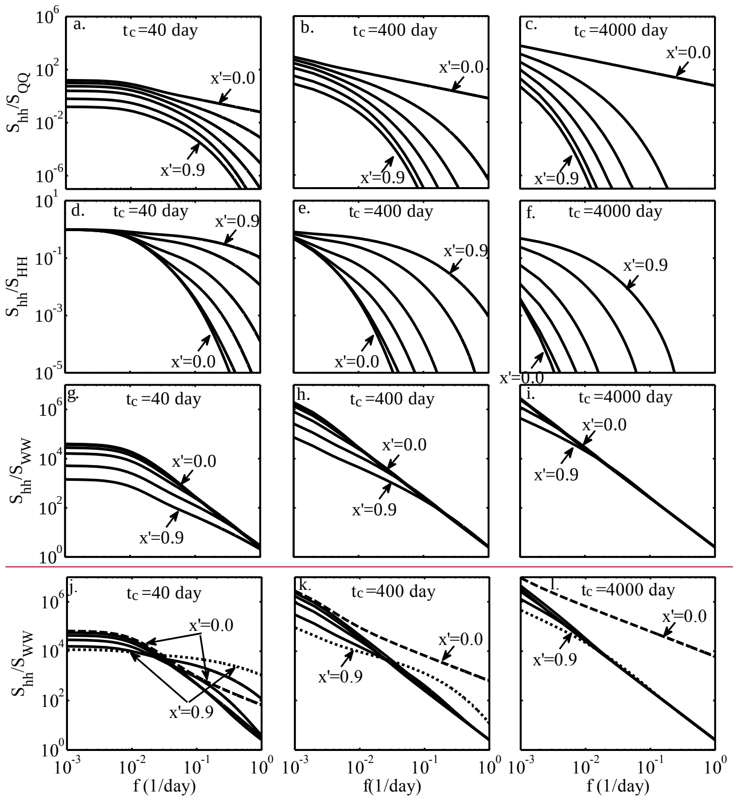

Figure 3

~~Figure captions~~

~~**Figure 1** A schematic of the unconfined aquifer studied where W(t) is the time-dependent random source/sink, $H_0(x)$ is the random initial condition, Q(t) is the random time-dependent flux at the left boundary, H(t) is the random time-dependent water level at the right boundary, L [L] is distance from the left to the right boundary, and h(x, t) is the random groundwater level in the aquifer.~~

~~**Figure 2** The graphs on the left column (five graphs) are the standard deviation (σ'_h) of groundwater level ($h(x, t)$) versus the dimensionless time (t') at the dimensionless locations x'=0.0, 0.2, 0.4, 0.6, and 0.8. The graphs on the right~~

带格式的：居中

带格式的：居中，缩进：左侧： 0 厘米，悬挂缩进： 1.33 字符，首行缩进： -1.33 字符，定义网格后自动调整右缩进，行距：1.5 倍行距，到齐到网格

column (five graphs) are σ'_h versus x' for the different t': b) and d) are for t'= 0.0, 0.2, 0.4, 0.6 and 0.8, f) and h) are for t'=0.01, 0.1, and 1.0, and j) is for t'=0.01, 0.2, 0.4, 0.6 and 0.8. Also, a) and b) are based on Eq.(11) where $\sigma_W^2 = \sigma_Q^2 = \sigma_H^2 = 0$; c) and d) are based on Eq. (12) where $\sigma_{W_0}^2 = \sigma_Q^2 = \sigma_H^2 = 0$; e) and f) are based on Eq. (13) where $\sigma_{W_0}^2 = \sigma_W^2 = \sigma_H^2 = 0$; g) and h) are based on Eq. (14) where $\sigma_{W_0}^2 = \sigma_W^2 = \sigma_Q^2 = 0$; i) and j) are based on Eq.(15) where $\sigma_{W_0}^2 \neq \sigma_W^2 \neq \sigma_Q^2 \neq \sigma_H^2 \neq 0$.

Figure 3 The dimensionless power spectrum versus frequency (f) at the dimensionless locations x'=0.0, 0.2, 0.4, 0.6, 0.8, and 0.9. The graphs on the left column are for t_c = 40 day, the graphs on the middle column are for t_c = 400 day, and the graphs on the right column are for t_c = 4000 day. The graphs on the first row are the dimensionless spectrum S_{hh}/S_{QQ} when $S_{WW}=0$, $S_{HH}=0$, and $S_{QQ}\neq 0$ in Eq. (10), the graphs on the second row is S_{hh}/S_{HH} when $S_{WW}=0$, $S_{QQ}=0$, and $S_{HH}\neq 0$, the graphs on the third row are S_{hh}/S_{WW} when $S_{QQ}=0$, $S_{HH}=0$, and $S_{WW}\neq 0$, and the graphs on the bottom row is S_{hh}/S_{WW} when $S_{QQ}\neq 0$, $S_{HH}\neq 0$, and $S_{WW}\neq 0$.

带格式的：字体：(中文) 黑体

带格式的：字体：(中文) 黑体

带格式的：字体：(中文) 黑体

带格式的：字体：(中文) 黑体

带格式的：字体：(中文) 黑体

带格式的：字体：(中文) 黑体

带格式的：字体：(中文) 黑体

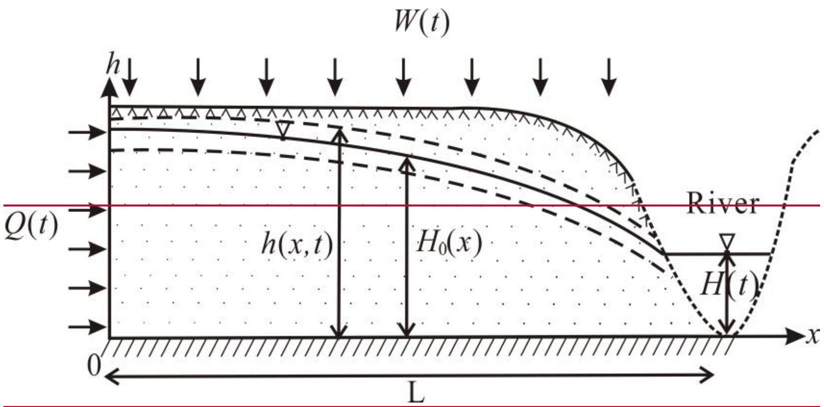

Figure 1 ~~A schematic of the~~ unconfined aquifer ~~studied where W(t) is the time-dependent random source/sink, $H_0(x)$ is the random initial condition, Q(t) is the random time-dependent flux at the left boundary, H(t) is the random time-dependent water level at the right boundary, L [L] is distance from the left to the right boundary, and h(x, t) is the random groundwater level in the aquifer.~~

带格式的：居中

~~**Figure 1** The standard deviation (σ'_h) of *h(x, t)* versus the dimensionless time (t') at the dimensionless locations *x'*=0.0, 0.2, 0.4, 0.6, and 0.8 (the four graphs in the left column) and the standard deviation (σ'_h) of *h(x, t)* versus the dimensionless location (x') for the dimensionless time *t'*=0.01, 0.1, and 1.0 (the four graphs in the right column): a) and b) are based on Eq.(11) where $\sigma_W^2 = \sigma_Q^2 = \sigma_H^2 = 0$; c) and d) are based on Eq. (12) where $\sigma_{W_0}^2 = \sigma_Q^2 = \sigma_H^2 = 0$; e) and f) are based on Eq. (13) where $\sigma_{W_0}^2 = \sigma_W^2 = \sigma_H^2 = 0$; g) and h) are based on Eq. (14) where $\sigma_{W_0}^2 = \sigma_W^2 = \sigma_Q^2 = 0$.~~

带格式的：居中，缩进：左侧： 0 厘米，悬挂缩进： 1.33 字符，首行缩进： -1.33 字符，定义网格后自动调整右缩进，行距：1.5 倍行距，到齐到网格

~~**Figure 2** a) The standard deviation (σ'_h) of *h(x, t)* versus the dimensionless time (t') at the dimensionless locations *x'*=0.0, 0.2, 0.4, 0.6, and 0.8 and b) the standard deviation (σ'_h) of *h(x, t)* versus the dimensionless location (x') for the dimensionless time t'=0.01, 0.1, and 1.0, evaluated based on Eq.(15) where $\sigma_{W_0}^2 \neq \sigma_W^2 \neq \sigma_Q^2 \neq \sigma_H^2 \neq 0$.~~

~~**Figure 3** The dimensionless power spectrum versus frequency (*f*) at the dimensionless locations *x'*=0.0, 0.2, 0.4, 0.6, 0.8, and 0.9. The left column is for t_c = 40 day, the middle column is for t_c = 400 day, and the right column is for t_c = 4000 day. The first row is the dimensionless spectrum S_{hh}/S_{QQ} when $S_{WW}=0$, $S_{HH}=0$, and $S_{QQ}\neq 0$ in Eq. (10), the second row is S_{hh}/S_{HH} when $S_{WW}=0$, $S_{QQ}=0$, and $S_{HH}\neq 0$, and the bottom row is S_{hh}/S_{WW} when $S_{QQ}=0$, $S_{HH}=0$, and $S_{WW}\neq 0$.~~

~~**Figure 4** The dimensionless power spectrum versus frequency (*f*) at the dimensionless locations *x'*=0.0, 0.2, 0.4, 0.6, 0.8, and 0.9 when $S_{QQ}\neq 0$, $S_{HH}\neq 0$, and $S_{WW}\neq 0$ for a)~~

~~t_e = 40 day, b) t_e = 400 day, and c) t_e = 4000~~

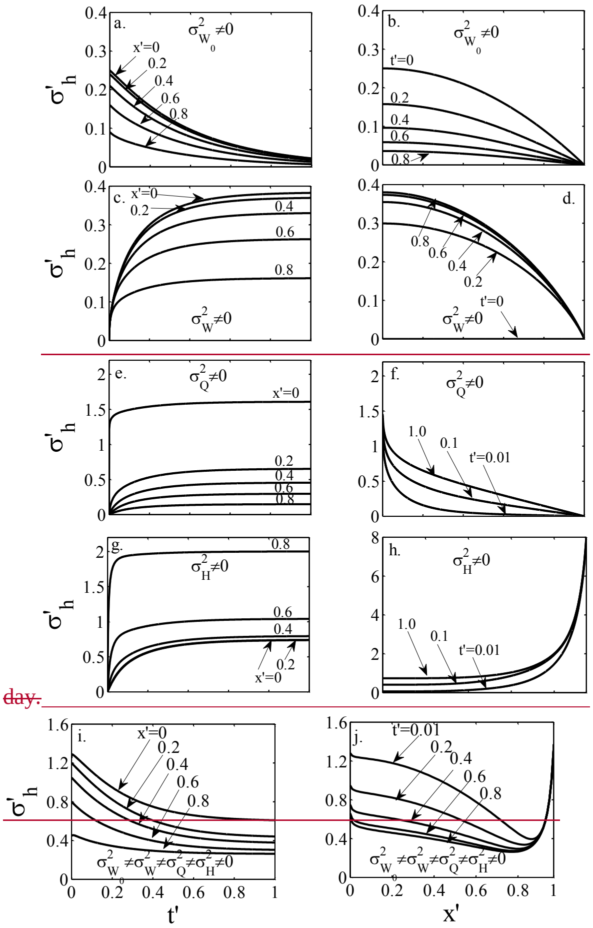

~~day.~~

~~**Figure 2** The graphs on the left column (five graphs) are the standard deviation (σ'_h) of groundwater level ($h(x, t)$) versus the dimensionless time (t') at the dimensionless locations x'=0.0, 0.2, 0.4, 0.6, and 0.8. The graphs on the right column (five graphs) are σ'_h versus x' for the different t': b) and d) are for t'= 0.0, 0.2, 0.4, 0.6 and 0.8, f) and h) are for t'=0.01, 0.1, and 1.0, and j) is for t'=0.01, 0.2, 0.4, 0.6 and 0.8. Also, a) and b) are based on Eq.(11) where $\sigma_W^2 = \sigma_Q^2 = \sigma_H^2 = 0$; c) and d) are based on Eq. (12) where $\sigma_{W_0}^2 = \sigma_Q^2 = \sigma_H^2 = 0$;~~

~~e) and f) are based on Eq. (13) where~~ $\sigma^2_{W_0} = \sigma^2_W = \sigma^2_H = 0$~~; g) and h) are based on Eq. (14) where~~ $\sigma^2_{W_0} = \sigma^2_W = \sigma^2_Q = 0$~~; i) and j) are based on Eq.(15) where~~ $\sigma^2_{W_0} \neq \sigma^2_W \neq \sigma^2_Q \neq \sigma^2_H \neq 0$~~.~~

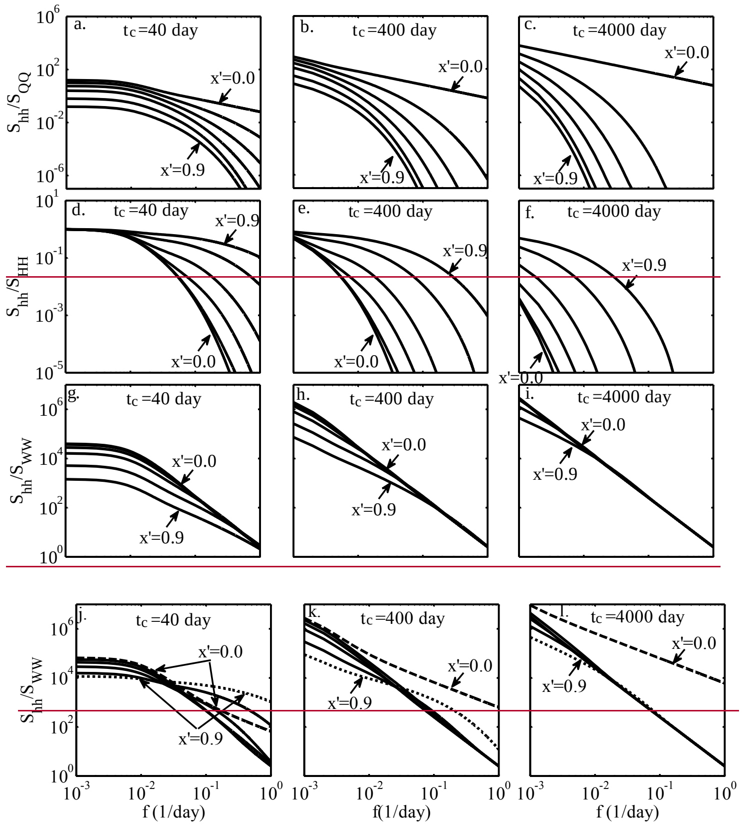

~~**Figure 3** The dimensionless power spectrum versus frequency (*f*) at the dimensionless locations *x'*=0.0, 0.2, 0.4, 0.6, 0.8, and 0.9. The graphs on the left column are for t_c = 40 day, the graphs on the middle column are for t_c = 400 day, and the graphs on the right column are for t_c = 4000 day. The graphs on the first row are the dimensionless spectrum~~ S_{hh}/S_{QQ} ~~when~~ $S_{WW}=0$~~,~~ $S_{HH}=0$~~, and~~ $S_{QQ}\neq 0$ ~~in Eq. (10), the graphs on the second row is~~ S_{hh}/S_{HH} ~~when~~ $S_{WW}=0$~~,~~ $S_{QQ}=0$~~, and~~ $S_{HH}\neq 0$~~, the graphs on the third row~~

带格式的：字体：（中文）黑体

~~are~~ $\cancel{S_{hh}/S_{WW}}$ ~~when~~ $\cancel{S_{QQ}=0}$ ~~,~~ $\cancel{S_{HH}=0}$ ~~, and~~ $\cancel{S_{WW}\neq 0}$ ~~, and the graphs on the bottom row is~~

$\cancel{S_{hh}/S_{WW}}$ ~~when~~ $\cancel{S_{QQ}\neq 0}$ ~~,~~ $\cancel{S_{HH}\neq 0}$ ~~, and~~ $\cancel{S_{WW}\neq 0}$ ~~.~~

带格式的：字体：(中文) 黑体

带格式的：字体：(中文) 黑体
带格式的：字体：(中文) 黑体
带格式的：字体：(中文) 黑体
带格式的：字体：(中文) 黑体
带格式的：字体：(中文) 黑体